Monthly Notices
of the
ROYAL ASTRONOMICAL SOCIETY

Mon. Not. R. Astron. Soc. **416,** 178–204 (2011) doi:10.1111/j.1365-2966.2011.19020.x

Constraining the properties of 1.2-mm dust clumps that contain luminous water masers

S. L. Breen[1,2]★ and S. P. Ellingsen[2]

[1]*CSIRO Astronomy and Space Science, PO Box 76, Epping, NSW 1710, Australia*
[2]*School of Mathematics and Physics, University of Tasmania, Private Bag 37, Hobart, TAS 7001, Australia*

Accepted 2011 May 6. Received 2011 May 6; in original form 2011 March 28

ABSTRACT

We have conducted a sensitive water maser search with the Australia Telescope Compact Array towards 267 1.2-mm dust clumps presented in the literature. We combine our new observations with previous water maser observations to extend our sample to 294 1.2-mm dust clumps, towards which we detect 165 distinct water maser sites towards 128 1.2-mm dust clumps. Within the fields of our observations, we additionally find four water masers with no apparent associated 1.2-mm dust continuum emission. Our overall detection rate of 44 per cent appears to vary as a function of Galactic longitude. We find that there is an excellent correspondence between the locations of the detected water masers with the peak of the target 1.2-mm dust clump sources. As expected from previous similar studies, the water masers are chiefly detected towards the bigger, brighter and more massive 1.2-mm dust clumps.

We find further evidence to suggest that the water masers tend to increase in flux density (and therefore luminosity), as well as velocity range, as the sources evolve. We also show that the current sample of water maser sources suffers less from evolutionary biases than previous targeted searches.

We have compared the locations of the water masers with dust clumps which have a previously determined association with 6.7-GHz methanol masers and 8-GHz radio continuum. We find that the fraction of 1.2-mm dust clump sources in our sample that are associated only with water masers (41) is higher than that of the sources associated only with methanol masers (13). This suggests that water masers can be present at an even earlier evolutionary stage than 6.7-GHz methanol masers. Comparison of the water maser detection rates associated with different combinations of methanol maser and radio continuum, as well as those with neither tracer, shows that the highest detection rate is towards those sources which also exhibit methanol maser emission.

We have tested a previously hypothesized model for water maser presence towards 1.2-mm dust clumps. We not only find water masers towards a high proportion of the clumps that the model predicts would have associated water masers, but also find a number of water masers towards sources with a low calculated probability. We propose that this is likely an artefact of the poorly determined distances to the sources. We suggest refinements and future work which will further constrain the nature of the driving sources associated with water masers.

Key words: masers – stars: formation – ISM: molecules – radio lines: ISM.

1 INTRODUCTION

To date there have been relatively few large-scale, unbiased surveys for water masers. Instead, searches have focused on high-mass star formation regions, typically targeting regions selected on the basis of *IRAS* colours (e.g. Churchwell, Walmsley & Cesaroni 1990; Codella et al. 1995; Sunada et al. 2007) or other maser species (e.g. Batchelor et al. 1980; Caswell et al. 1983; Beuther et al. 2002). Due to this, the known sample of water masers lacks the completeness that has been achieved for both 6.7-GHz methanol masers (e.g. Caswell et al. 2010; Green et al. 2010) and main-line OH masers (e.g. Caswell 1998). This, coupled with the fact that the positions of the majority of Southern hemisphere water masers are not known to subarcsec accuracy, means that relatively little is known about the nature of sources that are able to produce luminous water masers.

★E-mail: Shari.Breen@csiro.au

Large-scale, unbiased surveys for water masers are hindered by the large amounts of time required and the susceptibility of their observation to poor weather conditions. Further complications arise from the intrinsic variability of the sources which requires high positional precision in either the initial observations, or rapid follow-up observations. Some systematic searches for water masers have been attempted (e.g. Matthews et al. 1985; Breen et al. 2007; Caswell & Breen 2010; Caswell, Breen & Ellingsen 2011) but generally cover only very small regions of the Galactic plane. However, the observations of a relatively shallow but large-scale single-dish survey for water masers have recently been completed, covering 100° in longitude of the southern Galactic plane (Walsh et al. 2008), and the survey results are expected in the coming year.

Due to the difficulties associated with complete searches, attempts have been made to model water maser presence towards high-mass star formation regions, with the aim of gaining a more complete sample of water maser sources. These attempts have used particular observable properties of the high-mass star formation regions to make these predictions. Palla et al. (1991) modelled the probability of water maser presence on the basis of *IRAS* far-infrared colours. This model was tested by Palla et al. (1993) and resulted in a detection rate of around 5 per cent. This disappointing result is most likely due to the poor spatial resolution of the *IRAS* observations (30 arcsec at 100 μm) which results in significant source confusion in crowded high-mass star formation regions, demonstrating the need for high-resolution complementary data in the formulation of such models.

A systematic search for water masers of almost half a square degree of the G 333.2−0.6 giant molecular cloud (GMC; Breen et al. 2007) revealed a strong relationship between water maser presence and the bigger, brighter, more massive and dense 1.2-mm dust clumps (identified by Mookerjea et al. 2004), within the GMC. From these observations, Breen et al. (2007) produced what appears to be a reliable statistical model for predicting which 1.2-mm dust clumps will and will not have an associated water maser. While the likelihood of water maser presence increases with increasing values of all dust clump properties tested, the simplest model with the greatest predictive properties was found to only include the dust clump radius. This model predicts that all 1.2-mm dust clumps of radius 1.25 pc (or higher) have a probability of 0.5 (or higher) of having an associated water maser.

While the model presented in Breen et al. (2007) is promising, the water maser survey observations on which this model was derived were of comparatively low sensitivity (detection limit of ∼5 Jy or more in some regions). This, combined with the fact that the sample size was small, means that its validity cannot be determined before testing and refining it on a much larger sample. A reliable model relating the properties of 1.2-mm dust clumps to the presence/absence of water masers represents a unique tool for investigating questions such as the mass range of the stars that produce luminous water masers and the evolutionary phase they trace. Here we perform the necessary observations to test and refine the model developed in Breen et al. (2007).

Hill et al. (2005) present a catalogue of 404 1.2-mm dust clumps, a large but manageable sample, perfect for a targeted water maser search to test the current model. Hill et al. (2005) targeted their 1.2-mm dust continuum observations towards 131 regions that were suspected of undergoing massive star formation, using the presence of previously identified methanol masers and/or ultracompact H II (UCHII) regions to select their targets. The observations were carried out using the SIMBA instrument on the 15-m Swedish ESO Submillimetre Telescope (SEST) and detected emission directly associated with all but 20 of the methanol masers and nine of the UCHII regions targeted. Hill et al. (2005) also made a large number of serendipitous detections within the target fields.

Here we present new Australia Telescope Compact Array (ATCA) observations towards 267 of the Hill et al. (2005) dust clumps and supplement our observations with data taken from the literature (Forster & Caswell 1989; Breen et al. 2010b; Caswell & Breen 2010). Altogether, we present water maser data towards 294 dust clump. Using the model of Breen et al. (2007) we find that few of these dust clumps have high calculated probabilities of water maser presence (only 58 have probabilities greater than 0.01).

Breen et al. (2010a) present 12.2-GHz methanol maser observations targeting a number of these dust sources. This search for 12.2-GHz methanol masers constitutes a near-complete sample within the sample of Hill et al. (2005) sources, since no strong 12.2-GHz emission is expected in regions lacking 6.7-GHz methanol maser emission. Since a number of the sources presented in Hill et al. (2005) are contained within the regions searched for OH maser emission by Caswell (1998), a large subset of the 1.2-mm dust clumps have been searched for OH masers.

2 OBSERVATIONS AND DATA REDUCTION

2.1 Observations

The feasibility of this study was tested with observations using the University of Tasmania's 26-m Mount Pleasant radio telescope. All 404 1.2-mm dust clumps given in Hill et al. (2005) were targeted in these observations during 2007. An estimated 150 water maser sources were detected within the regions. An effort was made to locate the origin of the emissions by observing four-point grids around each of the targets and fitting a 2D Gaussian to the relative amplitudes of the emission detected in each. Given the immense success in detecting water maser sources, together with the impossible task of confidently disentangling nearby sources and associating them with the 1.2-mm dust clumps (especially given the limited pointing accuracy of the instrument), we proposed to observe the sources with the ATCA. Using the ATCA has several advantages, foremost of which is the ability to obtain accurate positions and gain much greater sensitivity.

Successful ATCA observations were carried out in three different array configurations over four epochs; these are listed in Table 1. For 137 of the 404 1.2-mm continuum sources observed by Hill et al. (2005), observations at 22 GHz are not presented. The reasons for the omission of these 137 sources were chiefly due to (i) their proximity to a declination of 0° (where observations can be particularly troubling at the ATCA), (ii) their location in the Northern hemisphere, (iii) their lack of reported dust characteristics or (iv) because the weather conditions they were taken in were too poor to result in reliable data. Observations of an additional 27 1.2-mm dust clumps were not necessary since they are associated with water masers reported to good positional accuracy in the literature.

Table 1. ATCA observations: epochs, array configurations and typical synthesized beam sizes.

Array	Epoch	Beam size
H75	2007 October 9, 10	28 × 24
H214	2007 December 7	13 × 8
H214	2008 July 12, 13	13 × 8
6B	2008 August 15, 16, 17	1.7 × 0.5

In total, we successfully searched 267 1.2-mm dust clumps for water maser presence with the ATCA. For all observations the field of view of the telescope is almost 5 arcmin, and the full width at half-maximum (FWHM) of the primary beam is 2.3 arcmin. Observations were carried out in groups of sources in the same neighbourhood so as to decrease overheads and allow reference pointing observations to be carried out efficiently. Pointings were carried out on a strong continuum source, located within $\sim 20^\circ$ of the target sources, approximately every hour. Using this method, the pointing is usually accurate to 5 arcsec, compared to about 20 arcsec when no pointing observations are carried out.

Targets were observed in a series of cuts, interspersed with phase calibration observations. At all epochs of observations only a single linearly polarized signal was recorded. The general observation strategy differed depending on the array and weather conditions, but, in general, nearby sources were grouped together and bracketed by phase calibration observations carried out on a compact continuum source, located not more than 10° from the targets. The time spent observing the targets and the time between phase calibrations was tailored to most efficiently observe the targets in the allocated time on the ATCA. The average strategy was to observe each target field for 10 min, over five cuts, with phase calibration (onsource for 1.5 min) carried out every 10 min. In general, these observations have allowed 5σ detections to be made at the 150–200 mJy level in the central section of the beam. For some sources, integration times were adjusted depending on the scheduled time allotment, and due to this the sensitivity limit may be either slightly lower or slightly higher (these are listed in column 10 of Table 2).

On each observing day, observations of a bandpass calibrator were completed. Two different sources were used: PKS B1253−055 and PKS B1921−293; both are strong at 22 GHz and are usefully observable at high elevations near the beginning and end of the time that the Galactic plane is visible, respectively. Primary flux calibration is with respect to observations of PKS B1934−638, which were also carried out daily.

Details of the observations carried out in each of the array configurations are given below. Descriptions of the correlator configurations (and therefore spectral resolution and velocity coverage) and individual observation strategies are also given in this section.

2.1.1 H75

The first series of observations were carried out in the most compact ATCA configuration, H75. Primarily, observations of sources located near declination zero were intended for this array configuration, but we were able to observe some additional, early rising sources in a Director's time allocation prior to our scheduled time on 2007 October 9.

For these observations, the correlator was configured to record 1024 channels across a bandwidth of 16 MHz for a single polarization. This correlator configuration allowed for a channel spacing of 0.21 km s^{-1}, corresponding to a velocity resolution of 0.25 km s^{-1}. The velocity coverage of these observations was just over 200 km s^{-1}.

In these observations, target sources were observed for 10 min each, over a series of five cuts (in general) spread over several hours. Observations of a phase calibrator source were carried out every 8–14 min.

2.1.2 H214

Water maser observations were carried out in the H214 hybrid configuration over two epochs. The first epoch was during 2007 December 7 and included only one source (G 213.705−12.597) which was observed as part of a multifrequency study of the masers associated with nearby star formation region Mon R2. The adopted correlator configuration for these observations were very different for this source, using a bandwidth of 4 MHz and 1024 channels. In this configuration the velocity coverage is limited to ~ 50 km s^{-1}, but the spectral resolution is increased to 0.06 km s^{-1}.

The main series of observations carried out in this array configuration were completed in 2008 July. For these observations the correlator was configured to record 512 channels over a bandwidth of 32 MHz for a single polarization. We made this change in correlator configuration, as from our first series of observations, it was clear that for some sources we were unable to observe the full extent of the velocity range of the emission. In these observations we made a sensible compromise, forgoing additional spectral resolution for twice the bandwidth. The resultant velocity coverage is over 400 km s^{-1}, and the spectral resolution is 1.0 km s^{-1}. The average strategy for these observations was to observe each source for 12–14 min over six to seven cuts of 2 min each spaced over several hours. Phase calibrator observations were completed approximately every 13 min.

2.1.3 6B

The final series of observations was carried out in a 6B array in 2008 August. The correlator was configured as for the observations carried out in the H214 array, giving a velocity coverage of more than 400 km s^{-1} and a spectral resolution of 1.0 km s^{-1}. Similar to the other observations, the observing strategy for observations in this array saw sources observed as a series of 2-min cuts spaced over several hours. On average, sources were observed seven times, giving onsource integration times of 14 min. Observations of a phase calibrator were conducted approximately every 7 min.

2.2 Data reduction

All ATCA data were reduced using the MIRIAD software package (Sault, Teuben & Wright 1995), applying the standard techniques for ATCA spectral line observations. Image cubes of the entire primary beam and usable velocity range were produced for each source. The flux densities of sources that were located away from the centre of the primary beam have been corrected to account for beam attenuation using the MIRIAD task 'linmos'. Both vector and scalar average spectra of the calibrated *uv*-data were inspected for each of the targets and cross-checked with the emission identified in each of the image cubes. Spectra for each of the detected sources were produced by integrating the emission in the image cubes. The typical resultant rms noise in each spectrum was 25–40 mJy for sources located near the centre of the beam.

The typical synthesized beam sizes experienced in each of the array configurations are listed in Table 1. In both of the hybrid configurations (H75 and H214), data from the 6-km antenna (antenna 6) were not included in the data reduction. The adopted water maser rest frequency was 22 235.079 85 MHz.

3 RESULTS

Hill et al. (2005) presented a catalogue of 404 1.2-mm dust clumps. Towards 294 of these clumps, we present water maser data and compare our detections with the derived probability of water maser presence (using the model presented in Breen et al. 2007). Most of the water maser data presented are new observations (132 of 165 water masers); however, where appropriate, data from

Table 2. Target 1.2-mm dust clumps, probability of water maser association, followed by a description of the water maser observations including any detections. Columns (1)–(3) give the 1.2-mm dust clump name followed by the right ascension and declination (Hill et al. 2005) and column (4) shows the calculated probability of water maser presence (using the model derived by Breen et al. 2007). Column (5) gives information about the ATCA array configuration used in the water maser observations followed by the epoch. In some cases, data are taken from Breen et al. (2010b), which are marked in column (5) with a 'BCEP' followed by the year of the observations. This format is also followed for sources taken from Caswell & Breen (2010) (CB) and Forster & Caswell (1989) (FC). Columns (6)–(13) give details of the water masers detected towards the dust clumps (which in some cases is more than one source), as well as 5σ detection limits where no source is detected. Specifically, column (6) gives the water maser Galactic coordinates, column (7) the water maser right ascension, column (8) the water maser declination, column (9) the separation between water maser and 1.2-mm dust clump peak (arcsec), column (10) the water maser peak flux density (Jy) or if preceded by '<' the 5σ detection limit (mJy), column (11) the velocity of the water maser peak emission (km s^{-1}), column (12) the velocity range of either the detected emission or the observed velocity range if no detection and column (13) the integrated flux density of the water maser emission (Jy km s^{-1}). Column (14) presents notes related to the sources, which in most cases are further discussed in Section 3.1 [Note the following abbreviations: BS(RS) indicates that the source is dominated by a blueshifted (redshifted) feature.].

Dust clump					Water maser								
Name (l, b) (degrees)	RA (J2000) ($^{h}m^{s}$)	Dec. (J2000) ($^{\circ}\,'\,''$)	Prob.	Array and epoch	Name (l, b) (degrees)	RA (J2000) ($^{h}m^{s}$)	Dec. (J2000) ($^{\circ}\,'\,''$)	Sep. (arcsec)	Sp (Jy)	Vp	Vr	Int	Notes
G 213.61−12.6	06 07 47.9	−06 22 57	3.7E−4	H214dec07	G 213.705−12.597	06 07 47.85	−06 22 56.6	1	92	12	4, 13	78	Mon R2
G 269.45−1.47	09 03 13.5	−48 55 22	0.15	H214jul08	G 269.461−1.471	09 03 15.01	−48 55 31.4	18	0.6	51	49, 52	1.6	
				H214jul08	G 269.457−1.467	09 03 14.87	−48 55 12.6	24	0.8	66	56, 69	1.7	
G 269.15−1.13	09 03 32.3	−48 28 00	1.2E−4	H214jul08	G 269.153−1.128	09 03 33.52	−48 28 03.0	12	26	7	6, 16	40	
G 270.25+0.84	09 16 41.4	−47 55 46	4.1E−5	H214jul08	G 270.254+0.835	09 16 41.13	−47 56 11.3	25	98	9	4, 17	199	
				H214jul08	G 270.257+0.834	09 16 41.62	−47 56 17.4	31	60	8	−2, 48	227	
G 284.271−0.391	10 23 47.0	−57 48 38	8.5E−5	H214jul08					<155		−200, 150		
G 284.307−0.376	10 24 04.0	−57 49 02	1.5E−3	H214jul08					<155		−200, 150		
G 284.338−0.417	10 24 06.0	−57 52 06	5.4E−5	H214jul08					<400		−200, 150		
G 284.35−0.42	10 24 10.0	−57 52 39	1.4E−4	H214jul08	G 284.351−0.418	10 24 10.92	−57 52 33.9	9	233	7	−32, 61	847	
G 284.345−0.404	10 24 12.0	−57 51 42	1.5E−4	H214jul08					<280		−200, 150		
G 284.341−0.389	10 24 14.0	−57 50 46	5.8E−3	H214jul08					<215		−200, 150		
G 284.328−0.365	10 24 15.0	−57 49 10	4.9E−5	H214jul08	G 284.329−0.365	10 24 15.27	−57 49 09.4	2	0.8	1	−5, 1	1.7	
G 284.384−0.441	10 24 18.0	−57 54 46	1.4E−4	H214jul08					<185		−200, 150		
G 284.344−0.366	10 24 21.0	−57 49 42	1.5E−4	H214jul08					<156		−200, 150		
G 284.352−0.353	10 24 27.0	−57 49 18	1.9E−3	H214jul08					<200		−200, 150		
G 287.37+0.65	10 48 05.2	−58 26 40	3.1E−4	H214jul08	G 287.372+0.644	10 48 04.59	−58 27 01.4	22	5	−1	−21, 7	12	
G 290.40−2.91	10 57 33.0	−62 58 54	9.4E−5	H214jul08	G 290.411−2.914	10 57 34.20	−62 59 02.4	12	12	−13	−32, 8	100	
G 291.256−0.769	11 11 33.9	−61 21 22	1.8E−4	6Baug08	G 291.257−0.767	11 11 34.56	−61 21 16.8	7	2.1	−27	−28, −1	6.4	
				6Baug08	G 291.254−0.768	11 11 32.89	−61 21 14.9	10	1.7	−29	−29, −23	2.4	
G 291.256−0.743	11 11 38.3	−61 19 54	3.7E−4	6Baug08	G 291.256−0.739	11 11 39.22	−61 19 42.6	12	11	−25	−26, −24	13	
G 291.27−0.70	11 11 54.8	−61 18 26	0.046	H214jul08	G 291.274−0.709	11 11 53.46	−61 18 24.3	10	61	−32	−53, −4	148	
				H214jul08	G 291.271−0.719	11 11 49.82	−61 18 53.8	45	218	−94	−101, −19	705	BS
G 291.288−0.706	11 12 00.6	−61 18 34	1.6E−4	H214jul08	G 291.284−0.716	11 11 56.68	−61 19 00.9	57	730	−128	−136, −108	3789	Clump edge, BS
G 291.302−0.693	11 12 09.4	−61 18 10	1.8E−4	6Baug08					<304		−200, 150		
G 291.309−0.681	11 12 15.0	−61 17 38	7.0E−4	6Baug08	G 291.314−0.680	11 12 17.21	−61 17 44.2	17	8.4	−29	−32, −22	16	
G 290.37+1.66	11 12 16.1	−58 46 19	9.4E−5	BCEP03	G 290.374+1.661	11 12 17.98	−58 46 21.6	15	3.5	−12	−20, −10		
				BCEP03	G 290.384+1.663	11 12 22.53	−58 46 29.0	51	6	−38	−50, −35		
G 291.587−0.499	11 14 54.5	−61 13 32	0.69	6Baug08					<128		−200, 150		
G 291.576−0.468	11 14 57.8	−61 11 40	8.3E−3	6Baug08					<267		−200, 150		
G 291.572−0.450	11 14 58.9	−61 10 36	3.1E−4	6Baug08					<247		−200, 150		
G 291.608−0.532	11 15 01.1	−61 15 56	0.19	BCEP03	G 291.610−0.529	11 15 02.58	−61 15 48.8	12	18	13	−66, 20		
G 291.597−0.496	11 15 02.2	−61 13 40	0.59	6Baug08					<128		−200, 150		
G 291.58−0.53	11 15 06.4	−61 09 38	5.3E−3	6Baug08	G 291.579−0.431	11 15 05.77	−61 09 39.5	6	120	11	−2, 16	776	Spread ∼2 arcsec
				6Baug08	G 291.579−0.434	11 15 05.19	−61 09 49.9	15	14.3	16.6	16, 20	30	

Table 2 – *continued*

Dust clump					Water maser								
Name (*l*, *b*) (degrees)	RA (J2000) ($^{h\,m\,s}$)	Dec. (J2000) ($^{\circ}\,'\,''$)	Prob.	Array and epoch	Name (*l*, *b*) (degrees)	RA (J2000) ($^{h\,m\,s}$)	Dec. (J2000) ($^{\circ}\,'\,''$)	Sep. (arcsec)	Sp (Jy)	Vp	Vr	Int	Notes
G 291.630−0.545	11 15 08.9	−61 17 08	0.89	BCEP03	G 291.629−0.541	11 15 08.88	−61 16 54.8	13	70	11	8, 16		
G 291.614−0.443	11 15 19.9	−61 11 08	5.9E−5	6Baug08	G 291.618−0.442	11 15 21.82	−61 11 09.3	14	0.7	15	0, 15	2.4	Slightly spread
				6Baug08	G 291.614−0.446	11 15 19.45	−61 11 15.2	8	0.3	7	7, 8	0.2	
G 293.824−0.762	11 32 01.4	−62 13 18	2.3E−3	H214jul08					<1065		−200, 150		
G 293.82−0.74	11 32 06.1	−62 12 22	6.3E−3	H214jul08	G 293.828−0.746	11 32 05.88	−62 12 26.1	4	1.5	59	15, 68	9	
G 293.892−0.782	11 32 32.4	−62 15 42	2.3E−4	H214jul08					<115		−200, 150		
G 293.95−0.8	11 32 42.0	−62 22 35	0.017	H214jul08	G 293.951−0.894	11 32 43.38	−62 23 07.1	34	15	35	29, 51	28	
G 293.942−0.876	11 32 42.0	−62 21 55	0.012	H214jul08					<120		−200, 150		
G 293.989−0.936	11 32 55.8	−62 26 11	0.038	H214jul08	G 293.993−0.931	11 32 58.42	−62 25 57.6	23	4.3	46	45, 48	7	
G 294.52−1.60	11 35 31.0	−63 14 36	2.0E−5	H214jul08	G 294.512−1.621	11 35 32.44	−63 14 42.8	12	49	−14	−19, −9	182	
G 294.945−1.737	11 38 57.1	−63 28 46	2.4E−5	H214jul08					<710		−200, 150		
G 294.97−1.7	11 39 09.0	−63 28 38	4.1E−5	H214jul08	G 294.977−1.734	11 39 14.25	−63 29 05.2	44	3.9	−7	−18, 3	15	
G 294.989−1.720	11 39 22.1	−63 28 30	2.6E−5	H214jul08	G 294.990−1.719	11 39 23.18	−63 28 27.5	8	25	−3	−12, −2	38	
G 298.26+0.7	12 11 45.4	−61 45 42	2.6E−4	H214jul08	G 298.259+0.748	12 11 46.72	−61 45 47.5	11	0.2	16	−29, 16	0.3	
G 299.02+0.1	12 17 18.6	−62 28 40	0.035	H214jul08	G 299.013+0.128	12 17 24.65	−62 29 04.4	48	106	19	−3, 30	164	
G 299.024+0.130	12 17 30.2	−62 29 04	2.3E−3	H214jul08					<184		−200, 150		
G 300.455−0.190	12 29 37.3	−62 57 23	0.014	H214jul08					<157		−200, 150		
G 300.51−0.1	12 30 02.0	−62 56 35	5.4E−3	H75oct07	G 300.504−0.176	12 30 03.60	−62 56 48.3	27	153	11	−37, 16	421	
G 301.14−0.2	12 35 29.1	−63 01 32	0.010	H214jul08	G 301.136−0.226	12 35 34.92	−63 02 31.0	72	322	−50	−72, −23	1606	Spread 5 arcsec
G 302.03−0.06	12 43 32.1	−62 55 06	3.4E−4	6Baug08					<111		−200, 150		
G 305.145+0.208	13 10 40.5	−62 34 53	4.5E−5	H214jul08					<159		−200, 150		
G 305.137+0.069	13 10 42.0	−62 43 13	1.0E−4	H214jul08	G 305.136+0.069	13 10 41.53	−62 43 12.7	3	1.2	−39	−40, −39	1.3	
				H214jul08	G 305.138+0.067	13 10 42.59	−62 43 20.4	8	4.2	−38	−39, −37	6	
				H214jul08	G 305.141+0.065	13 10 44.21	−62 43 27.3	21	0.5	−16	−71, −15	0.7	
G 305.201+0.241	13 11 08.3	−62 32 37	2.2E−5	H214jul08					<169		−200, 150		
G 305.202+0.230	13 11 09.4	−62 33 17	2.8E−4	H214jul08					<158		−200, 150		
G 305.20+0.02	13 11 12.3	−62 44 57	1.2E−3	H214jul08					<180		−200, 150		
G 305.192−0.006	13 11 13.6	−62 47 29	8.5E−5	BCEP03	G 305.191−0.006	13 11 12.95	−62 47 27.7	5	25	31	28, 36		
G 305.21+0.21	13 11 14.1	−62 34 45	0.02	H214jul08	G 305.208+0.206	13 11 13.60	−62 34 41.5	4	96	−39	−53, −30	425	
G 305.197+0.007	13 11 15.9	−62 46 41	1.8E−3	H214jul08	G 305.199+0.007	13 11 16.72	−62 46 37.6	7	16	−39	−42, 1	40	
G 305.200+0.02	13 11 17.0	−62 45 53	4.1E−5	H214jul08					<314		−200, 150		
G 305.226+0.275	13 11 19.8	−62 30 29	1.1E−4	6Baug08	G 305.223+0.275	13 11 18.50	−62 30 30.6	9	0.9	−36	−47, −34	2.8	
G 305.228+0.286	13 11 20.9	−62 29 48	3.4E−5	6Baug08					<115		−210, 140		
G 305.238+0.261	13 11 26.7	−62 31 16	5.9E−4	6Baug08					<110		−210, 140		
G 305.248+0.245	13 11 32.5	−62 32 12	1.6E−4	6Baug08	G 305.251+0.251	13 11 33.94	−62 31 47.2	27	0.8	−39	−42, −36	1.5	
G 305.233−0.023	13 11 35.8	−62 48 16	1.4E−4	6Baug08					<105		−210, 140		
G 305.269−0.010	13 11 54.4	−62 47 19	8.5E−4	CB07	G 305.269−0.003	13 11 53.82	−62 46 55.6	24	0.8	−60	−83, −53		
G 305.358+0.203	13 12 31.6	−62 34 11	6.9E−3	6Baug08	G 305.359+0.200	13 12 32.12	−62 34 21.0	11	5	−85	−95, 54	39	BS
G 305.362+0.185	13 12 34.7	−62 35 15	4.5E−4	6Baug08	G 305.366+0.184	13 12 36.75	−62 35 14.8	14	1.1	−17	−17, −16	1.1	
G 305.361+0.151	13 12 35.2	−62 37 15	9.4E−5	6Baug08	G 305.362+0.150	13 12 35.87	−62 37 18.9	6	120	−35	−41, −31	280	
G 305.37+0.21	13 12 36.3	−62 33 39	4.1E−4	6Baug08	G 305.368+0.212	13 12 36.21	−62 33 34.4	5	25	−33	−88, 39	64	Spread 2 arcsec
				6Baug08	G 305.369+0.212	13 12 37.04	−62 33 35.5	6	0.35	7	5, 7	0.4	
G 305.340−0.172	13 12 38.1	−62 36 42	1.0E−4	6Baug08					<360		−210, 140		

Table 2 – *continued*

Dust clump					Water maser							
Name (*l*, *b*) (degrees)	RA (J2000) ($^{h\,m\,s}$)	Dec. (J2000) ($^{\circ}\,'\,''$)	Prob.	Array and epoch	Name (*l*, *b*) (degrees)	RA (J2000) ($^{h\,m\,s}$)	Dec. (J2000) ($^{\circ}\,'\,''$)	Sep. (arcsec)	Sp (Jy)	Vp	Vr	Int	Notes
G 305.520−0.020	13 14 06.1	−62 46 41	5.9E−5	6Baug08					<135		−210, 140		
G 305.549+0.002	13 14 20.0	−62 45 13	2.8E−4	6Baug08					<112		−210, 140		
G 305.552+0.013	13 14 21.2	−62 44 33	1.6E−4	6Baug08					<162		−210, 140		
G 305.552+0.012	13 14 22.4	−62 46 01	1.3E−3	6Baug08	G 305.553−0.012	13 14 22.79	−62 45 59.4	3	1.1	−44	−44, −7	3.8	
G 305.561+0.012	13 14 25.8	−62 44 32	4.8E−3	CB07	G 305.561+0.013	13 14 25.68	−62 44 30.0	2	0.7	−42	−48, −38		
G 305.581+0.033	13 14 35.1	−62 43 02	5.3E−3	6Baug08					<113		−210, 140		
G 305.605+0.010	13 14 49.1	−62 44 24	1.8E−4	6Baug08					<111		−210, 140		
G 305.81−0.25	13 16 43.2	−62 58 37	1.0E−3	BCEP03	G 305.799−0.245	13 16 42.92	−62 58 31.7	6	400	−26	−45, 35		
G 305.833−0.196	13 16 58.3	−62 55 25	2.0E−4	6Baug08					<126		−210, 140		
G 306.33−0.3	13 21 18.2	−63 00 43	4.5E−5	BCEP03	G 306.318−0.331	13 21 20.87	−63 00 22.7	27	2.1	−19	−24, −14		
G 306.319−0.343	13 21 18.2	−63 01 07	1.8E−5	H75oct07					<133		−10, −190		
G 306.343−0.302	13 21 32.3	−62 58 26	2.0E−5	6Baug08					<156		−200, 150		
G 306.345−0.345	13 21 34.6	−62 59 54	2.0E−5	H75oct07	G 306.341−0.321	13 21 32.33	−62 59 36.9	23	0.7	−20	−22, −14	0.6	
G 309.917+0.494	13 50 38.2	−61 34 20	6.5E−5	6Baug08					<137		−200, 150		
G 309.92+0.4	13 50 41.6	−61 35 15	0.025	6Baug08					<137		−200, 150		
G 318.913−0.162	15 00 33.6	−58 58 05	4.9E−5	6Baug08	G 318.916−0.164	15 00 35.18	−58 58 06.4	19	0.2	−45	−46, −18	0.5	
G 318.92−0.68	15 00 55.3	−58 58 54	5.4E−5	BCEP04	G 318.948−0.196a	15 00 55.18	−58 58 51.6	3	9	−36	−44, −27		
				BCEP04	G 318.948−0.196b	15 00 55.33	−58 58 53.6	1	7	−38	−39, −21		
G 323.74−0.3	15 31 41.6	−56 30 11	1.6E−4	BCEP03	G 323.740−0.263	15 31 45.48	−56 30 49.6	50	140	−50	−72, −46		
G 330.95−0.18	16 09 48.8	−51 53 51	0.28	BCEP03	G 330.954−0.182	16 09 52.65	−51 54 54.6	73	240	−80	−150, 70		
G 332.640−0.586	16 19 30.5	−51 02 40	3.4E−5	6Baug08					<144		−150, 200		
G 332.648−0.606	16 19 38.1	−51 03 12	0.16	6Baug08	G 332.654−0.614	16 19 38.53	−51 03 38.3	26	1.4	−56	−57, −52	2.8	
				6Baug08	G 332.653−0.621	16 19 43.50	−51 03 36.6	57	40	−45	−52, −44	42	
G 332.73−0.62	16 20 02.7	−51 00 32	2.4E−5	6Baug08	G 332.725−0.621	16 20 02.95	−51 00 32.3	2	5	−8	−52, −5	8	
G 332.777−0.584	16 20 07.0	−50 56 48	3.1E−5	6Baug08					<143		−150, 200		
G 332.627−0.511	16 20 07.0	−51 00 00	2.6E−5	6Baug08	G 332.737−0.620	16 20 05.92	−51 00 00.5	10	0.4	−52	−54, −51	0.7	
G 332.794−0.598	16 20 15.0	−50 56 40	6.5E−5	6Baug08					<143		−150, 200		
G 0.204+0.051	17 45 54.3	−28 44 08	9.1E−3	6Baug08					<126		−150, 200		
G 0.49+0.19	17 46 03.9	−28 24 58	5.9E−5	6Baug08	G 0.496+0.188	17 46 03.99	−28 24 51.7	6	0.5	0	−4, 28	2.4	
				6Baug08	G 0.497+0.188	17 46 03.98	−28 24 50.1	8	1.0	−8	−13, 0	3.6	
G 0.266−0.034	17 46 07.1	−28 41 28	9.1E−3	6Baug08					<131		−150, 200		
G 0.21−0.00	17 46 07.7	−28 45 20	0.025	BCEP04	G 0.209−0.002	17 46 07.44	−28 45 32.1	13	2.2	39	18, 42		
				BCEP04	G 0.212−0.002	17 46 07.86	−28 45 23.0	4	0.9	56	55, 56		
G 0.497+0.170	17 46 08.2	−28 25 23	4.5E−5	6Baug08					<113		−150, 200		
G 0.24+0.01	17 46 09.5	−28 43 36	0.91	6Baug08					<120		−150, 200		
G 0.527+0.181	17 46 10.1	−28 23 31	9.4E−5	6Baug08	G 0.527+0.181	17 46 10.00	−28 23 30.9	1	1.0	−1	−42, 0	1.2	
G 0.271+0.022	17 46 10.7	−28 41 36	3.3E−3	6Baug08					<131		−150, 200		
G 0.26+0.01	17 46 11.4	−28 42 40	1.0	6Baug08	G 0.261+0.016	17 46 10.63	−28 42 17.6	25	1.5	37	35, 38	2.5	
G 0.83+0.18	17 46 52.8	−28 07 35	1.8E−4	6Baug08	G 0.837+0.183	17 46 53.35	−28 07 34.3	7	0.5	−39	−39, −38	0.8	
				6Baug08	G 0.835+0.184	17 46 52.80	−28 07 35.8	1	1	6	−32, 7	5	
G 0.331−0.164	17 47 00.0	−28 45 20	1.6E−3	6Baug08					<116		−150, 200		
G 0.310−0.170	17 47 01.2	−28 45 36	9.4E−5	6Baug08	G 0.306−0.170	17 47 00.60	−28 45 45.4	12	0.6	11	10, 12	0.7	
G 0.32−0.20	17 47 09.1	−28 46 16	1.0	BCEP04	G 0.316−0.201	17 47 09.29	−28 46 15.5	3	22	23	14, 31		

Table 2 – *continued*

Dust clump					Water maser								
Name (*l*, *b*) (degrees)	RA (J2000) ($^{h\,m\,s}$)	Dec. (J2000) ($^{\circ}\,'\,''$)	Prob.	Array and epoch	Name (*l*, *b*) (degrees)	RA (J2000) ($^{h\,m\,s}$)	Dec. (J2000) ($^{\circ}\,'\,''$)	Sep. (arcsec)	Sp (Jy)	Vp	Vr	Int	Notes
G 0.325−0.242	17 47 20.1	−28 47 04	7.8E−5	6Baug08					<115		−150, 200		
G 1.124−0.065	17 48 31.6	−28 00 31	2.2E−3	6Baug08					<240		−150, 200		
G 1.134−0.073	17 48 34.7	−28 00 16	3.1E−4	6Baug08					<240		−150, 200		
G 1.105−0.098	17 48 36.4	−28 02 31	4.1E−4	6Baug08					<137		−150, 200		
G 1.13−0.11	17 48 41.9	−28 01 44	1.0	6Baug08	G 1.127−0.106	17 48 41.38	−28 01 38.7	9	5	−23	−24, −21	12	
G 1.14−0.12	17 48 48.5	−28 01 13	0.077	6Baug08	G 1.147−0.124	17 48 48.53	−28 01 11.3	2	43	−20	−23, −8	137	
G 0.55−0.85	17 50 14.5	−28 54 31	7.0E−4	6Baug08	G 0.546−0.851a	17 50 14.44	−28 54 30.1	1	499	34	15, 44	1164	
				6Baug08	G 0.546−0.851b	17 50 14.39	−28 54 29.7	2	30	13	−67, 105	280	
				6Baug08	G 0.546−0.851c	17 50 14.51	−28 54 30.8	0	29	18	15, 21	61	
G 0.549−0.868	17 50 18.8	−28 53 14	2.3E−4	6Baug08					<2645		−150, 200		
G 0.627−0.848	17 50 24.9	−28 50 15	3.4E−5	6Baug08	G 0.627−0.838	17 50 22.69	−28 49 57.2	18	0.4	124	124, 126	0.4	RS
G 0.600−0.871	17 50 26.7	−28 52 23	5.9E−05	6Baug08					<145		−150, 200		
G 2.54+0.20	17 50 46.5	−26 39 45	4.4E−4	BCEP04	G 2.536+0.198	17 50 46.66	−26 39 44.9	2	30	25	−1, 63		
G 5.48−0.24	17 59 04.6	−24 20 55	0.36	6Baug08					<136		−150, 200		
G 5.504−0.246	17 59 07.5	−24 19 19	0.046	6Baug08	G 5.513−0.255	17 59 10.25	−24 19 17.6	38	0.2	22	18, 23	0.4	On clump edge
G 5.89−0.39	18 00 31.0	−24 03 59	1.9E−3	BCEP03	G 5.886−0.392	18 00 30.52	−24 03 58.2	7	40	11	−10, 23		
G 5.90−0.42	18 00 40.9	−24 04 21	4.4E−4	BCEP04	G 5.901−0.430	18 00 40.95	−24 04 19.6	2	3.9	14	−40, 30		
G 5.90−0.44	18 00 43.9	−24 04 47	6.4E−4	BCEP04	G 5.897−0.445	18 00 43.90	−24 04 58.1	1	0.9	19	19, 20		
G 6.53−0.10	18 00 50.9	−23 21 29	0.77	BCEP04	G 6.534−0.105	18 00 49.44	−23 21 40.2	23	0.5	22	6, 23		
G 6.60−0.08	18 00 54.1	−23 17 02	1.1E−5	BCEP04	G 6.611−0.082	18 00 54.15	−23 17 00.8	1	7	6	−34, 11		
G 8.127+0.255	18 02 52.8	−21 47 54	1.1E−4	6Baug08					<130		−140, 210		
G 8.138+0.246	18 02 56.2	−21 47 38	1.5E−3	6Baug08					<130		−140, 210		
G 8.13+0.22	18 03 00.8	−21 48 10	1.9E−3	6Baug08					<4256		−140, 210		
G 5.948−1.125	18 03 26.3	−24 22 29	5.4E−5	6Baug08	G 5.947−1.127	18 03 26.61	−24 22 35.7	8	5	8	6, 10	7	
G 5.975−1.146	18 03 34.5	−24 21 41	3.4E−5	6Baug08					<135		−140, 210		
G 5.971−1.158	18 03 36.8	−24 22 13	7.8E−5	6Baug08					<135		−140, 210		
G 5.97−1.17	18 03 40.9	−24 22 37	4.1E−4	6Baug08					<248		−140, 210		
G 10.10+0.73	18 05 15.6	−19 50 55	1.4E−5	6Baug08					<129		−140, 210		
G 9.62+0.19	18 06 14.8	−20 31 37	7.0E−4	BCEP03	G 9.620+0.194	18 06 14.97	−20 31 37.5	2	25	5	−30, 50		
				BCEP03	G 9.622+0.195	18 06 14.88	−20 31 31.0	6	1.4	21	0, 22		
G 8.68−0.36	18 06 18.9	−21 37 21	0.046	6Baug08	G 8.672−0.354	18 06 18.85	−21 37 19.9	1	8	3	−17, 5	39	
				6Baug08	G 8.669−0.356a	18 06 19.04	−21 37 31.7	11	5	25	23, 26	8	
				6Baug08	G 8.670−0.356	18 06 19.12	−21 37 29.7	9	1.2	31	30, 32	1.4	
				6Baug08	G 8.669−0.356b	18 06 18.94	−21 37 32.2	11	10	32	31, 35	20	
				6Baug08	G 8.667−0.357	18 06 18.95	−21 37 39.3	18	1.5	36	35, 41	2.4	
				6Baug08	G 8.669−0.356c	18 06 19.03	−21 37 31.8	11	3.3	42	38, 44	9	
G 8.686−0.366	18 06 23.5	−21 36 57	3.3E−3	6Baug08					<256		−140, 210		
G 8.644−0.395	18 06 24.6	−21 40 01	1.6E−4	6Baug08					<120				
G 8.713−0.364	18 06 26.4	−21 35 29	0.011	6Baug08					<123				
G 8.735−0.362	18 06 28.7	−21 34 17	0.010	6Baug08	G 8.732−0.368	18 06 29.70	−21 34 36.4	24	1.4	50	31, 52	6	
G 8.724−0.401a	18 06 36.1	−21 36 01	8.5E−5	6Baug08					<140		−140, 210		
				6Baug08	G 8.727−0.395	18 06 35.08	−21 35 38.6	*	1.1	36	36, 42	1.6	Dust not listed?
G 8.724−0.401b	18 06 36.7	−21 37 05	4.1E−4	6Baug08					<113		−140, 210		

Table 2 – *continued*

Dust clump					Water maser								
Name (l, b) (degrees)	RA (J2000) ($^{h}m^{s}$)	Dec. (J2000) ($^{\circ}\,'\,''$)	Prob.	Array and epoch	Name (l, b) (degrees)	RA (J2000) ($^{h}m^{s}$)	Dec. (J2000) ($^{\circ}\,'\,''$)	Sep. (arcsec)	Sp (Jy)	Vp	Vr	Int	Notes
G 8.718−0.410	18 06 37.3	−21 36 33	2.4E−5	6Baug08					<113		−140, 210		
G 9.966−0.020	18 07 45.8	−20 19 47	3.1E−5	6Baug08					<128		−140, 210		
G 9.99−0.03	18 07 50.4	−20 18 51	1.5E−3	6Baug08	G 9.986−0.028	18 07 50.12	−20 18 56.6	7	14	46	40, 60	38	
G 10.001−0.033	18 07 53.2	−20 18 19	1.1E−4	6Baug08					<108		−140, 210		
G 10.47+0.02	18 08 37.9	−19 51 41	0.99	BCEP03	G 10.473+0.027	18 08 38.30	−19 51 48.8	10	45	60	30, 93		
				BCEP03	G 10.480+0.034	18 08 37.69	−19 51 12.4	29	12	64	63, 65		Not in BCEP04
G 10.44−0.01	18 08 44.9	−19 54 38	7.6E−3	BCEP04	G 10.455−0.018	18 08 45.01	−19 54 35.1	3	6	71	58, 85		
G 10.287−0.110	18 08 45.9	−20 05 34	9.4E−5	6Baug08					<314		−140, 210		
G 10.284−0.126	18 08 49.4	−20 05 58	7.1E−5	6Baug08	G 10.288−0.125	18 08 49.42	−20 05 58.0	0	0.9	17	16, 18	1.1	
				6Baug08	G 10.287−0.125a	18 08 49.36	−20 05 58.6	1	1.6	13	13, 17	3.9	
				6Baug08	G 10.287−0.125b	18 08 49.28	−20 05 59.5	2	0.5	6	5, 7	0.7	
G 10.288−0.127	18 08 52.4	−20 05 58	5.4E−5	6Baug08					<110		−140, 210		
G 10.29−0.14	18 08 55.5	−20 05 58	2.3E−4	6Baug08					<209		−140, 210		
G 10.343−0.142	18 09 00.0	−20 03 34	3.1E−5	BCEP04	G 10.342−0.143	18 09 00.11	−20 03 35.8	2	4.8	8	−40, 61		
G 10.32−0.15	18 09 01.5	−20 05 08	7.7E−4	BCEP04	G 10.323−0.160	18 09 01.57	−20 05 07.6	1	3.2	−3	−6, 62		
G 10.146−0.314	18 09 14.2	−20 18 53	3.3E−3	6Baug08					<125		−140, 210		
G 10.191−0.307	18 09 18.2	−20 16 21	4.5E−5	6Baug08					<158		−140, 210		
G 10.148−0.331	18 09 18.2	−20 19 17	1.3E−3	6Baug08					<133		−140, 210		
G 10.214−0.305	18 09 20.5	−20 15 01	9.4E−5	6Baug08	G 10.215−0.305	18 09 20.72	−20 15 01.0	3	0.6	16	2, 8	2.6	
G 10.191−0.308	18 09 21.6	−20 16 21	4.5E−4	6Baug08					<158		−140, 210		
G 10.15−0.34	18 09 21.6	−20 19 25	0.099	6Baug08					<135		−140, 210		
G 10.213−0.326	18 09 25.0	−20 15 41	0.042	6Baug08					<268		−140, 210		
G 10.188−0.344	18 09 26.2	−20 17 33	0.025	6Baug08					<114		−140, 210		
G 10.133−0.378	18 09 26.7	−20 21 25	5.9E−4	6Baug08					<126		−140, 210		
G 10.164−0.360	18 09 26.7	−20 19 17	0.95	6Baug08	G 10.157−0.366	18 09 27.04	−20 19 49.2	34	0.7	−22	−24, −22	1.1	
G 10.237−0.328	18 09 28.4	−20 14 29	7.8E−5	6Baug08					<121		−140, 210		
G 10.206−0.350	18 09 29.6	−20 16 45	0.017	6Baug08					<269		−140, 210		
G 10.184−0.370	18 09 31.3	−20 18 29	1.0E−4	6Baug08					<184		−140, 210		
G 10.198−0.372	18 09 33.5	−20 17 49	5.9E−4	6Baug08					<141		−140, 210		
G 10.138−0.419	18 09 34.6	−20 22 21	1.5E−4	6Baug08					<128		−140, 210		
G 10.149−0.407	18 09 35.3	−20 21 25	4.9E−4	6Baug08					<128		−140, 210		
G 10.165−0.403	18 09 36.4	−20 20 29	4.5E−4	6Baug08					<142		−140, 210		
G 10.194−0.387	18 09 36.4	−20 18 29	5.8E−4	6Baug08					<192		−140, 210		
G 10.186−0.404	18 09 39.2	−20 19 25	5.4E−5	6Baug08					<142		−140, 210		
G 10.63−0.33B	18 10 15.7	−19 54 45	0.017	6Baug08					<123		−140, 210		
G 10.62−0.33	18 10 18.0	−19 54 05	0.042	6Baug08					<180		−140, 210		
G 9.88−0.75	18 10 19.0	−20 45 33	0.22	6Baug08	G 9.878−0.750	18 10 18.74	−20 45 38.4	7	0.9	31	23, 31	1.8	
G 9.924−0.749	18 10 24.1	−20 43 09	4.1E−4	6Baug08					<114		−140, 210		
G 10.62−0.38	18 10 29.4	−19 55 41	0.96	BCEP03	G 10.623−0.383	18 10 28.57	−19 55 49.4	14	350	2	−11, 5		
G 10.620−0.441	18 10 41.1	−19 57 41	1.4E−4	6Baug08					<114		−140, 210		
G 11.075−0.384	18 11 24.4	−19 32 04	7.7E−4	6Baug08					<115		−140, 210		
G 11.11−0.34	18 11 31.8	−19 30 44	0.27	6Baug08					<114		−140, 210		
G 11.117−0.413	18 11 35.8	−19 30 44	3.7E−4	6Baug08					<140		−140, 210		

Table 2 – *continued*

Dust clump					Water maser								
Name (*l*, *b*) (degrees)	RA (J2000) ($^{h\,m\,s}$)	Dec. (J2000) ($^{\circ}\,'\,''$)	Prob.	Array and epoch	Name (*l*, *b*) (degrees)	RA (J2000) ($^{h\,m\,s}$)	Dec. (J2000) ($^{\circ}\,'\,''$)	Sep. (arcsec)	Sp (Jy)	Vp	Vr	Int	Notes
G 12.88+0.48	18 11 51.4	−17 31 30	0.025	6Baug08	G 12.889+0.489	18 11 51.46	−17 31 28.9	1	8	29	28, 32	16	
G 11.948−0.003	18 11 52.9	−18 36 03	4.8E−3	6Baug08					<109		−140, 210		
G 12.914+0.493	18 11 53.6	−17 30 02	1.4E−4	6Baug08	G 12.915+0.493	18 11 53.74	−17 29 58.8	4	2.7	33	31, 34	3.9	
G 12.02−0.03	18 12 01.9	−18 31 56	6.4E−4	6Baug08					<120		−140, 210		
G 11.902−0.100	18 12 02.1	−18 40 26	5.4E−5	6Baug08					<118		−140, 210		
G 11.903−0.140	18 12 11.1	−18 41 27	0.027	BCEP03	G 11.903−0.142	18 12 11.41	−18 41 33.0	7	0.3	36	35, 38		Not in BCEP04
G 11.861−0.183	18 12 15.6	−18 44 58	4.5E−5	6Baug08					<121		−140, 200		
G 11.93−0.14	18 12 17.3	−18 40 03	2.3E−4	6Baug08					<178		−140, 200		
G 11.942−0.157	18 12 19.6	−18 39 54	3.2E−4	6Baug08	G 11.943−0.156	18 12 19.58	−18 39 52.0	2	4.9	41	7, 94	25	
G 12.200−0.003	18 12 23.5	−18 22 49	0.059	6Baug08	G 12.199−0.033	18 12 23.43	−18 22 50.7	2	0.2	51	51, 52	0.2	
G 11.956−0.177	18 12 25.7	−18 39 46	3.7E−5	6Baug08					<254		−140, 210		
G 12.20−0.09	18 12 39.2	−18 24 17	1.0	6Baug08	G 12.209−0.102a	18 12 39.89	−18 24 17.7	10	63	22	12, 29	199	
				6Baug08	G 12.209−0.102b	18 12 39.75	−18 24 17.7	8	75	0	−28, 50	462	
				6Baug08	G 12.209−0.101	18 12 39.69	−18 24 16.2	7	0.7	−32	−34, −31	1.4	
G 11.942−0.256	18 12 41.6	−18 24 47	2.1E−4	6Baug08	G 12.203−0.107	18 12 40.22	−18 24 47.4	1	1.1	33	28, 35	1.9	
G 12.18−0.12	18 12 42.7	−18 25 08	0.85	6Baug08					<208		−140, 210		
G 12.216−0.119	18 12 44.4	−18 24 25	0.023	6Baug08					<293		−140, 210		
G 11.99−0.27	18 12 51.2	−18 40 40	2.8E−4	6Baug08	G 11.991−0.272	18 12 51.20	−18 40 39.7	0	0.2	53	53, 54	0.2	
G 12.43−0.05	18 12 56.4	−18 11 04	0.98	6Baug08	G 12.429−0.048	18 12 54.41	−18 11 10.8	29	0.3	−72	−74, −38	2.1	BS
G 12.68−0.18	18 13 54.7	−18 01 41	0.30	H75oct07	G 12.681−0.182	18 13 54.73	−18 01 46.5	6	565	60	53, 64	668	
				H75oct07	G 12.670−0.177	18 13 52.42	−18 02 10.5	44	0.4	50	49, 50	0.1	
G 11.94−0.62B	18 13 58.5	−18 54 21	1.9E−3	6Baug08	G 11.918−0.613	18 13 58.12	−18 54 20.2	5	49	40	21, 45	122	
G 11.93−0.61	18 14 00.9	−18 53 27	2.3E−3	6Baug08					<149		−140, 210		
G 12.722−0.218	18 14 07.6	−18 00 37	1.9E−3	6Baug08	G 12.720−0.218	18 14 07.35	−18 00 42.7	7	0.6	−36	−36, −35	0.9	BS
G 12.885−0.222	18 14 28.3	−17 52 08	4.9E−5	6Baug08					<121		−140, 210		
G 12.892−0.226	18 14 30.0	−17 51 52	6.5E−5	6Baug08					<121		−140, 210		
G 12.90−0.25B	18 14 34.3	−17 51 56	2.1E−3	6Baug08	G 12.901−0.241	18 14 34.43	−17 51 51.8	5	2.2	36	24, 37	3.6	
G 12.859−0.272	18 14 36.1	−17 54 56	7.7E−4	6Baug08					<159		−140, 210		
G 13.87+0.28	18 14 36.1	−16 45 44	0.029	6Baug08	G 13.874+0.281	18 14 35.83	−16 45 35.9	9	39	−43	−47, −14	155	BS
G 12.90−0.26	18 14 39.5	−17 52 00	0.025	6Baug08	G 12.907−0.261	18 14 39.45	−17 52 06.8	7	1.1	28	26, 50	4.2	
				6Baug08	G 12.909−0.260	18 14 39.54	−17 52 00.0	1	2.2	27	26, 38	3.9	
G 12.878−0.226	18 14 41.7	−17 54 24	7.8E−5	6Baug08					<153		−140, 210		
G 12.897−0.281	18 14 42.9	−17 53 12	2.8E−5	6Baug08					<123		−140, 210		
G 12.914−0.280	18 14 44.5	−17 52 16	3.4E−5	6Baug08					<161		−140, 210		
G 12.938−0.272	18 14 45.7	−17 50 48	2.6E−5	6Baug08	G 12.939−0.271	18 14 45.58	−17 50 41.1	7	2.0	30	29, 37	7	
G 11.49−1.48	18 16 22.1	−19 41 27	1.1E−4	BCEP04	G 11.498−1.486	18 16 22.32	−19 41 26.1	3	112	17	−3, 21		
G 14.60+0.01	18 17 00.5	−16 14 44	1.3E−3	6Baug08	G 14.607+0.009	18 17 03.17	−16 14 41.6	40	2.5	27	4, 27	2.8	
				6Baug08	G 14.610+0.012	18 17 02.72	−16 14 28.0	36	0.6	8	8, 9	0.7	
				6Baug08	G 14.606+0.016	18 17 01.54	−16 14 32.1	19	0.5	21	17, 39	1.2	
				6Baug08	G 14.604+0.017	18 17 01.14	−16 14 38.8	11	9	30	20, 31	13	
G 10.84−2.59	18 19 12.6	−20 47 31	2.3E−4	6Baug08	G 10.843−2.593	18 19 12.51	−20 47 27.4	4	35	−81	−89, −73	127	BS
G 15.022−0.618	18 20 10.3	−16 10 35	4.9E−5	6Baug08					<231		−140, 210		
G 14.987−0.670	18 20 17.6	−16 13 55	3.7E−5	6Baug08					<124		−140, 210		

Table 2 – *continued*

Dust clump					Water maser								
Name (*l*, *b*) (degrees)	RA (J2000) ($^{h\,m\,s}$)	Dec. (J2000) ($^{\circ}\,'\,''$)	Prob.	Array and epoch	Name (*l*, *b*) (degrees)	RA (J2000) ($^{h\,m\,s}$)	Dec. (J2000) ($^{\circ}\,'\,''$)	Sep. (arcsec)	Sp (Jy)	Vp	Vr	Int	Notes
G 15.027−0.651	18 20 18.1	−16 11 15	1.6E−4	6Baug08	G 14.892−0.730	18 20 19.60	−16 10 38.4	43	4.3	25	20, 33	14	
G 15.054−0.641	18 20 19.2	−16 09 31	2.6E−5	6Baug08					<358		−140, 210		
G 14.983−0.687	18 20 20.9	−16 14 35	2.1E−4	6Baug08					<199		−140, 210		
G 15.012−0.671	18 20 20.9	−16 12 35	4.4E−4	6Baug08					<1000		−140, 210		
G 15.03−0.67	18 20 23.1	−16 11 16	1.9E−3	6Baug08	G 15.028−0.672	18 20 23.02	−16 11 47.8	32	4.2	21	18, 23	9	
G 14.99−0.70	18 20 23.1	−16 14 43	1.0E−4	6Baug08	G 14.985−0.696	18 20 23.16	−16 14 44.3	2	57	43	−20, 72	327	Spread
G 15.009−0.688	18 20 24.2	−16 13 15	4.2E−5	6Baug08					<235		−140, 210		
G 15.005−0.695	18 20 25.3	−16 13 39	3.7E−5	6Baug08					<400		−140, 210		
G 15.079−0.663	18 20 27.0	−16 08 51	1.0E−4	6Baug08					<171		−140, 210		
G 15.016−0.702	18 20 28.1	−16 13 15	3.4E−5	6Baug08					<400		−140, 210		
G 15.029−0.703	18 20 29.8	−16 12 35	2.8E−3	6Baug08					<400		−140, 210		
G 15.089−0.673	18 20 30.3	−16 08 35	1.1E−4	6Baug08					<118		−140, 210		
G 15.098−0.681	18 20 33.1	−16 08 19	5.4E−4	6Baug08					<173		−140, 210		
G 16.580−0.079	18 21 14.6	−14 32 52	9.3E−4	6Baug08					<124		−140, 210		
G 16.58−0.05	18 21 09.1	−14 31 49	3.3E−3	6Baug08	G 16.585−0.050a	18 21 09.05	−14 31 48.5	1	29	58	57, 68	117	
				6Baug08	G 16.585−0.050b	18 21 08.97	−14 31 47.6	2	4.6	71	57, 73	9	
G 18.087−0.292	18 24 56.0	−13 19 03	3.1E−5	H214jul08					<203		−120, 230		
G 18.095−0.299	18 24 58.6	−13 18 47	7.1E−5	H214jul08					<203		−120, 230		
G 18.105−0.304	18 25 00.8	−13 18 23	6.5E−5	H214jul08					<203		−120, 230		
G 18.112−0.321	18 25 05.1	−13 18 31	3.1E−5	H214jul08					<390		−120, 230		
G 19.61−0.1	18 27 16.3	−11 53 51	4.9E−4	H214jul08	G 19.613−0.134	18 27 16.60	−11 53 36.2	15	0.7	46	29, 60	1.6	
G 19.607−0.234	18 27 38.2	−11 56 38	9.3E−4	H214jul08	G 19.610−0.234	18 27 38.11	−11 56 35.4	3	90	42	−5, 81	477	Spread
G 21.87+0.01	18 31 02.1	−09 49 14	3.7E−5	H214jul08	G 21.880+0.014	18 31 01.77	−09 49 00.1	15	11	21	17, 29	35	
G 22.36+0.07B	18 31 43.2	−09 22 25	1.3E−3	H214jul08					<159		−120, 230		
G 22.35+0.06	18 31 44.1	−09 22 12	8.5E−4	H214jul08	G 22.357+0.066	18 31 44.11	−09 22 11.8	0	9	88	75, 90	31	
G 23.71+0.17	18 33 53.6	−08 07 15	2.8E−3	H214jul08	G 23.704+0.183	18 33 50.08	−08 07 15.2	52	0.6	111	111, 112	0.8	Clump edge
G 23.689+0.159	18 33 53.6	−08 08 43	8.5E−5	H214jul08					<203		−120, 230		
G 24.450+0.489	18 34 07.6	−07 19 05	3.7E−5	H214jul08					<214		−120, 230		
G 24.47+0.49	18 34 10.3	−07 17 45	8.3E−3	H214jul08					<186		−120, 230		
G 25.65+1.04	18 34 20.9	−05 59 40	9.3E−4	H214jul08	G 25.650+1.050	18 34 20.84	−05 59 42.2	2	131	41	−21, 56	321	
G 23.949+0.163	18 34 21.7	−07 54 45	5.9E−4	H214jul08	G 23.953+0.161	18 34 22.56	−07 54 37.4	15	0.4	48	41, 50	0.7	Clump edge
G 23.96+0.15	18 34 24.9	−07 54 53	4.8E−3	H214jul08	G 23.953+0.155	18 34 23.97	−07 54 48.2	15	0.8	66	65, 74	1.5	
G 23.281−0.201	18 34 25.4	−08 40 23	9.4E−5	H214jul08					<182		−120, 230		
G 23.268−0.210	18 34 25.9	−08 41 19	3.4E−4	H214jul08					<182		−120, 230		
G 24.012+0.173	18 34 26.5	−07 51 09	4.5E−5	H214jul08					<183		−120, 230		
G 23.976+0.150	18 34 27.6	−07 53 41	5.9E−5	H214jul08	G 23.980+0.149	18 34 28.17	−07 53 30.9	13	0.7	14	13, 15	1.2	
G 23.960+0.137	18 34 28.7	−07 54 53	1.6E−5	H214jul08					<243		−120, 230		
G 23.987+0.148	18 34 29.2	−07 53 09	8.5E−5	H214jul08					<244		−120, 230		
G 23.25−0.24	18 34 31.3	−08 42 47	7.1E−5	H214jul08	G 23.257−0.240	18 34 31.25	−08 42 46.0	1	1.0	78	72, 79	1.6	Spread
G 24.016+0.150	18 34 31.9	−07 51 33	2.4E−5	H214jul08					<216		−120, 230		
G 23.268−0.257	18 34 36.2	−08 42 39	1.6E−3	H214jul08					<187				
G 23.43−0.18	18 34 39.4	−08 31 33	0.016	H214jul08	G 23.436−0.184	18 34 39.25	−08 31 40.2	8	4.4	111	109, 112	7	
G 23.409−0.228	18 34 45.6	−08 34 21	1.8E−4	H214jul08					<3225		−120, 230		

Table 2 – *continued*

Dust clump					Water maser								
Name (*l*, *b*) (degrees)	RA (J2000) ($^{h\,m\,s}$)	Dec. (J2000) ($^{\circ}\,'\,''$)	Prob.	Array and epoch	Name (*l*, *b*) (degrees)	RA (J2000) ($^{h\,m\,s}$)	Dec. (J2000) ($^{\circ}\,'\,''$)	Sep. (arcsec)	Sp (Jy)	Vp	Vr	Int	Notes
G 23.420−0.235	18 34 48.4	−08 33 57	3.1E−4	H214jul08					<5000		−120, 230		
G 23.319−0.298	18 34 50.7	−08 41 03	4.1E−4	H214jul08	G 23.320−0.298	18 34 50.62	−08 41 00.1	3	0.2	99	98, 99	0.1	
G 23.754+0.095	18 36 06.1	−07 13 47	2.5E−3	H214jul08					<147		−120, 230		
G 24.792+0.099	18 36 09.4	−07 11 39	6.9E−3	H214jul08					<173		−120, 230		
G 24.78+0.08	18 36 12.6	−07 12 11	0.30	H214jul08	G 24.790+0.083	18 36 12.58	−07 12 11.6	1	54	113	35, 127	162	Spread
				H214jul08	G 24.792+0.082	18 36 13.13	−07 12 08.0	8	4.9	113	23, 151	39	
G 24.84+0.08	18 36 18.4	−07 08 52	6.4E−4	H214jul08	G 24.850+0.087	18 36 18.40	−07 08 50.6	1	0.9	106	106,116	2.5	Spread
G 24.850+0.082	18 36 19.5	−07 09 00	1.0E−4	H214jul08					<165		−120, 230		
G 24.919+0.088	18 36 25.9	−07 05 08	0.046	H214jul08	G 24.921+0.083	18 36 27.25	−07 05 10.3	20	1.4	84	82, 85	2.1	
				H214jul08	G 24.919+0.088	18 36 25.90	−07 05 08.1	0	6	42	35, 53	20	
G 25.802−0.159	18 38 57.0	−06 24 53	6.4E−4	H214jul08					<152		−120, 230		
G 25.83−0.18	18 39 03.6	−06 24 10	0.016	H214jul08	G 25.826−0.178	18 39 03.61	−06 24 10.3	0	38	95	80, 123	87	
G 28.14−0.00	18 42 42.6	−04 15 32	2.5E−3	H214jul08					<158		−120, 230		
G 28.20−0.04	18 42 58.1	−04 13 56	0.11	H75oct07	G 28.200−0.049	18 42 58.08	−04 13 57.7	2	8	96	57, 100	11	
G 28.198−0.063	18 43 00.8	−04 14 28	1.8E−4	H75oct07					<311		−30, 150		
G 29.193−0.073	18 43 02.4	−04 14 59	1.2E−4	H75oct07					<311		−30, 150		
G 28.28−0.35	18 44 14.2	−04 17 59	5.9E−4	H214jul08					<266		−120, 230		
G 28.31−0.38	18 44 22.0	−04 17 38	7.7E−4	H214jul08					<269		−120, 230		
G 29.888+0.001	18 45 52.8	−02 42 29	3.1E−5	H214jul08					<356		−120, 230		
G 29.889−0.006	18 45 54.4	−02 42 37	2.8E−4	H214jul08					<356		−120, 230		
G 29.918−0.014	18 45 59.7	−02 41 17	4.5E−5	H214jul08					<328		−120, 230		
G 29.86−0.04	18 46 00.2	−02 45 09	9.3E−4	H214jul08					<175		−120, 230		
G 29.861−0.053	18 46 01.3	−02 45 25	3.4E−4	H214jul08					<175		−120, 230		
G 29.853−0.062	18 46 02.4	−02 45 57	4.4E−4	H214jul08					<175		−120, 230		
G 29.96−0.02B	18 46 04.0	−02 39 25	0.30	H214jul08	G 29.955−0.016	18 46 03.74	−02 39 22.3	5	63	99	80, 115	340	
G 29.930−0.040	18 46 06.1	−02 41 25	4.1E−5	H75oct07					<7300		−30, 150		
G 29.9687−0.033	18 46 08.8	−02 39 09	4.1E−4	H75oct07					<374		−30, 150		
G 29.978−0.050	18 46 12.5	−02 39 09	0.016	H75oct07					<3035		−30, 150		
G 30.716−0.082	18 47 41.3	−02 00 33	2.1E−3	H75oct07	G 30.718−0.083	18 47 41.74	−02 00 29.5	7	2.2	96	91, 97	2.1	
G 35.02+0.35	18 54 00.5	+02 01 16	4.1E−4	FC89	G 35.025+0.250	18 54 00.59	+02 01 19.3	4	18.5	68.5			
G 35.575+0.010	18 56 13.5	+02 21 39	5.3E−3	H214jul08					<173		−120, 230		
G 35.574+0.007	18 56 14.0	+02 21 15	1.1E−3	H214jul08					<173		−120, 230		
G 35.58−0.03	18 56 22.4	+02 20 26	0.95	H75oct07	G 35.578−0.031	18 56 22.54	+02 20 27.4	3	12	52	42, 57	17	
G 35.585−0.026	18 56 22.4	+02 20 58	5.9E−4	H75oct07					<435		−30, 150		
G 35.564−0.037	18 56 22.4	+02 19 30	7.1E−5	H75oct07					<905		−30, 150		
G 35.601−0.018	18 56 22.4	+02 22 02	7.6E−3	H75oct07					<2005		−30, 150		
G 37.475−0.106	19 00 06.9	+03 59 39	1.2E−3	H214jul08	G 37.475−0.108	19 00 07.28	+03 59 34.7	7	0.2	52	51, 58	0.4	
G 37.55−0.11	19 00 16.0	+04 03 15	0.27	H214jul08					<105		−120, 230		

Breen et al. (2010b), Caswell & Breen (2010) and Forster & Caswell (1989) have been used to minimize repetition of observations.

Table 2 shows the targeted 1.2-mm dust clumps, along with their calculated probability of water maser presence, followed by the water maser data. We find a total of 165 water maser sources towards 128 of the 1.2-mm dust clumps. Spectra of each of the 132 water masers detected in our current observations are presented in Fig. 1 and are essentially ordered as the 1.2-mm dust clumps presented in Hill et al. (2005; in order of increasing right ascension) unless there was a need for nearby sources to be vertically aligned. For the majority of sources, a velocity range of 200 km s^{-1} is shown; however, this has been reduced to 100 km s^{-1} for sources observed in the H75 configuration of the ATCA (which were carried out with a smaller bandwidth), and for one source, G 213.705−12.597, a velocity range of 40 km s^{-1} is shown (this source was observed with 4-MHz bandwidth). Confusion from strong nearby sources are marked on the individual spectra, except where they are present as features of negative intensities. In some spectra, where confusing features from multiple nearby sources are present, we use an 'X' to indicate that those features are not associated with the presented source. A consequence of the relatively coarse spectral resolution of our observations, combined with the often strong and relatively narrow water maser features, is that 'ringing' is present in a number of spectra.

A number of the sources that we detect have been previously presented in the literature (e.g. Johnston et al. 1972; Caswell et al. 1974; Kaufmann et al. 1976; Genzel & Downes 1977; Batchelor et al. 1980; Braz & Scalise 1982; Braz & Epchtein 1983; Caswell et al. 1989; Hofner & Churchwell 1996, and references therein). However, the majority of these observations were conducted 20 or more years ago, with relatively poor positional accuracy. When combined with the often extreme variable nature of water maser sources, the task of identifying our sources with those in the literature is therefore fraught with difficulties. Since the only certain way to match up sources with those in the literature is by position, we only compare our detections with observations of comparable positional accuracy.

Several of the sources that we detect have been observed in interferometric observations (e.g. Forster & Caswell 1989; Caswell & Phillips 2008; Breen et al. 2010b; Caswell & Breen 2010), allowing us to compare our positions and therefore assess our positional uncertainties. In general, our positional agreement with previous observations is excellent, sometimes better than 0.5 arcsec, but consistently within 2 arcsec. Breen et al. (2010b) present a more extensive assessment of the positional uncertainties of their water maser observations carried out with the ATCA and conclude that perhaps the largest contributor to the uncertainty was the tendency for the water maser spots to be spread out and the difference between measuring a slightly different feature at a different epoch. Here we similarly find that this is the case, and therefore expect the positional uncertainties of the water masers that we present to be accurate to 2 arcsec.

Another facet of this assessment allowed us to determine the effect that the synthesized beam has on the positional accuracy of the sources. As can be seen in Table 1, the beam sizes resulting from the hybrid configurations are much larger than that of the more extended 6B array. Comparisons with other measurements shows that even when the beam is large, accurate positions can be derived, since it is rarely the case that two sources show emission at the same velocities and are spatially separated by less than a synthesized beam. The much smaller beam of the 6B array has allowed for some water maser sites to be broken up into individual components, although it is likely the case that very close companions are intimately associated with the same exciting source.

Notes on some individual sources are presented in Section 3.1. We find that there is an excellent correspondence between the locations of the detected water masers and the 1.2-mm dust sources, and this is discussed further in Section 4.3. In addition to the water masers that we detect towards 1.2-mm dust clumps, we detect four water maser sources that seem not to be associated with any dust continuum emission, and these are discussed in Section 3.2.

3.1 Individual sources

Here we draw attention to sources that we were unable to adequately describe in Table 2. Close neighbouring water masers are discussed, as well as sources with surprising velocities and intriguing histories. For some sources, associations with other maser species are also discussed.

G 213.705−12.597. This water maser is located in a nearby star formation region, Mon R2. Associated with this star formation region are many maser species, including 6.7- and 12.2-GHz methanol, main-line OH and some excited OH maser transitions. Of particular interest is the excited OH maser at the 4765-MHz transition; these sources are very rare (only about 20 known in the Galaxy), and this source is by far the strongest known at this transition. Furthermore, the emission from this 4765-MHz OH maser undergoes flaring activity that has not been seen in any other maser of this type (Smits, Cohen & Hutawarakorn 1998; Smits 2003).

G 284.351−0.418. This source is also presented in Breen et al. (2010b) as it is coincident with an OH maser (Caswell 1998), although it is named G 284.350−0.418, due to a slight difference in measured position affecting the rounded Galactic coordinates. In Breen et al. (2010b), spectra from two epochs are shown to display the typical level of variability seen in the water maser sources. When the 2003 and 2004 spectra are compared to our current observations, it can be seen that the source has once again varied by a moderate level and has increased in peak flux density by about a factor of 2.

G 291.271−0.719, G 291.274−0.709 and G 291.284−0.716. These three sources are also listed in Breen et al. (2010b) since they all fall within the field of a target OH maser source. Caswell & Phillips (2008) also observed this group of sources and remarked that the strongest source, G 291.284−0.716, is a member of a distinct class of sources that are dominated by strong blueshifted outflows. In fact, maser emission has never been detected at the systemic velocity of the source (to a limit of 0.3 Jy in these observations), which is around 100 km s^{-1} from the detected emission. The location of G 291.284−0.716 is very close to the edge of the 1.2-mm dust clump emission, unlike the majority of sources.

G 291.579−0.431 and G 291.579−0.434. G 291.579−0.431 shows emission spread over approximately 2 arcsec, and in Table 2 we present the median of the positions measured for the individual features. This source is clearly separated from G 291.579−0.434, which is located more than 10 arcsec away.

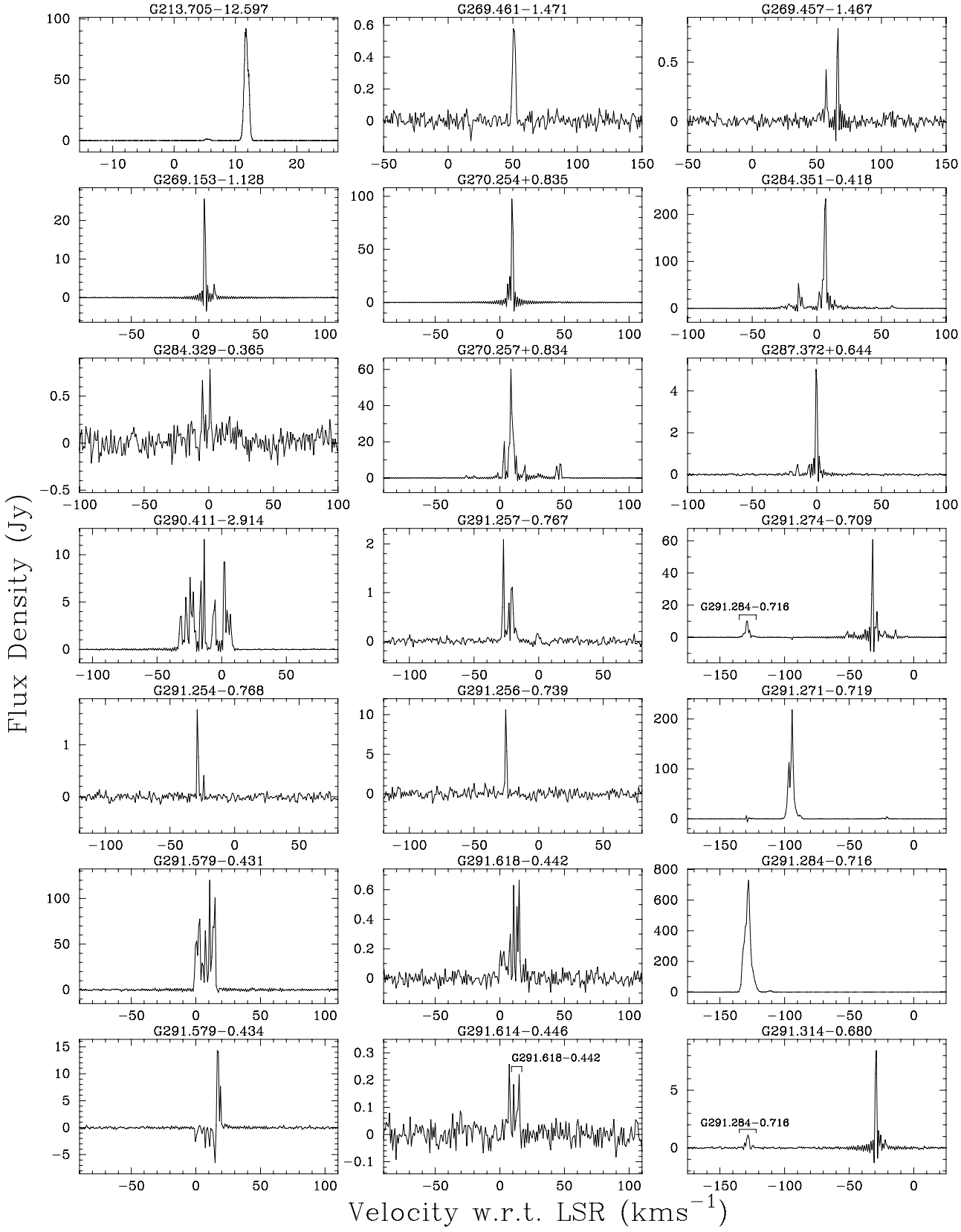

Figure 1. Spectra of the 22-GHz water masers detected towards 1.2-mm dust clumps.

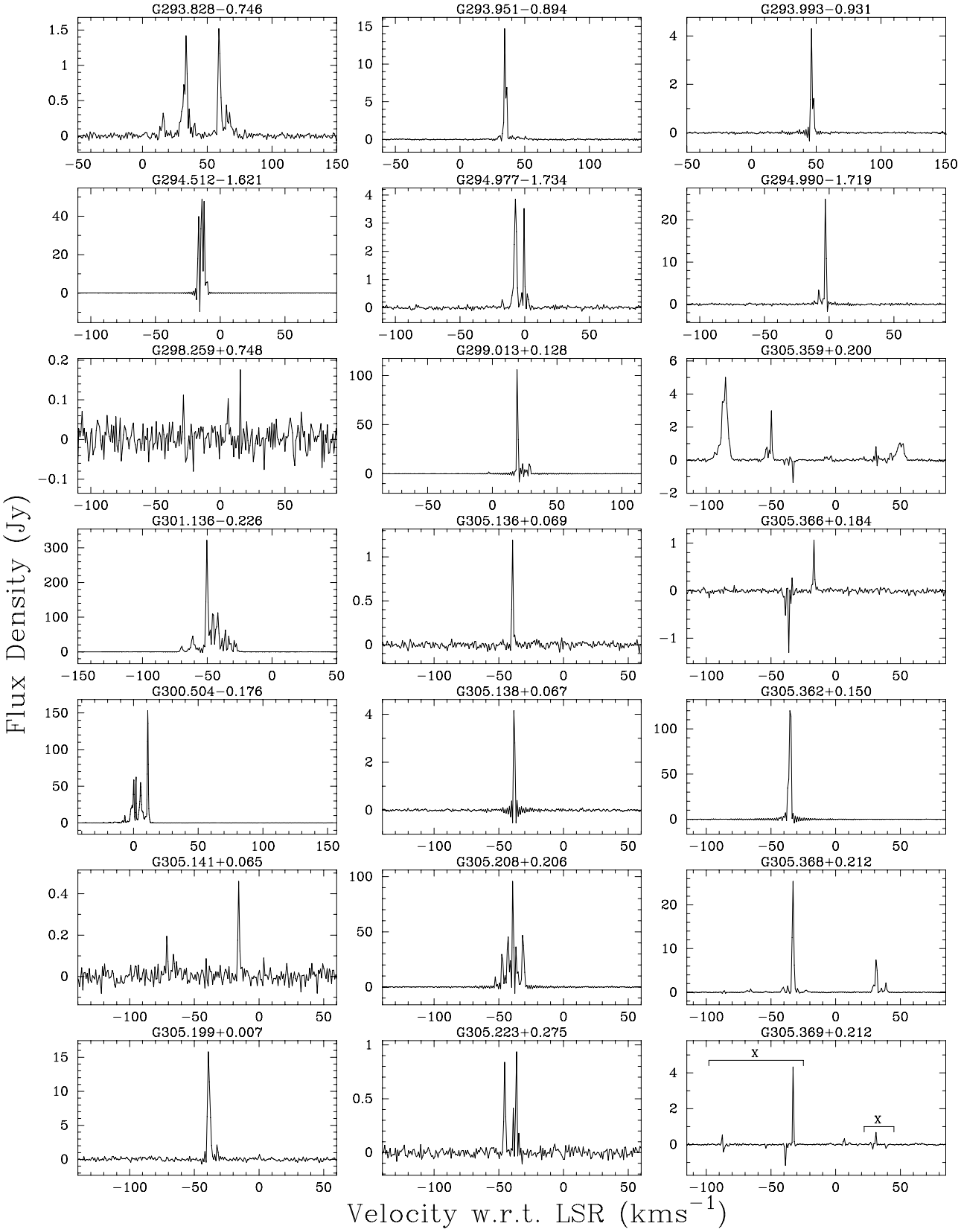

Figure 1 – *continued*

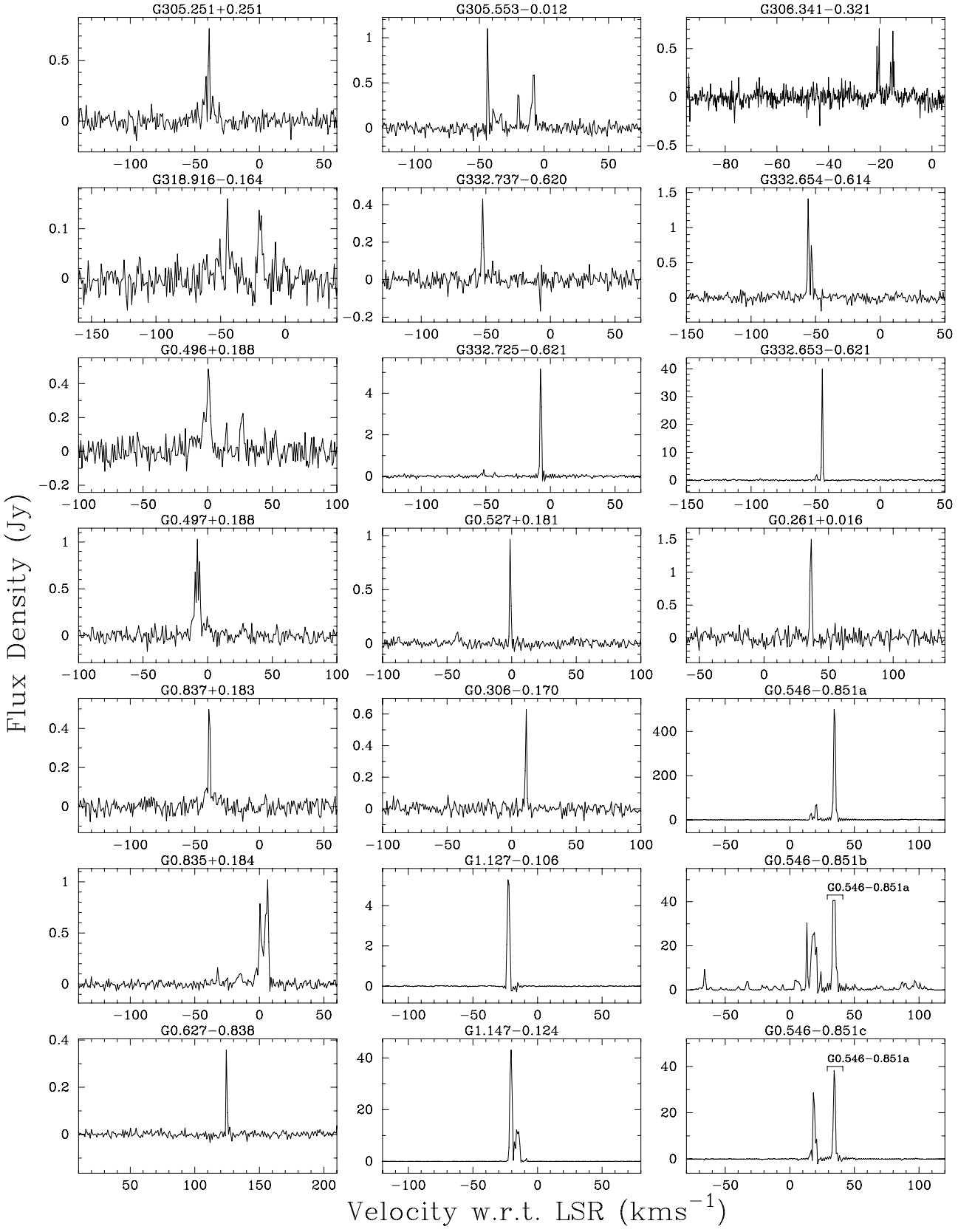

Figure 1 – *continued*

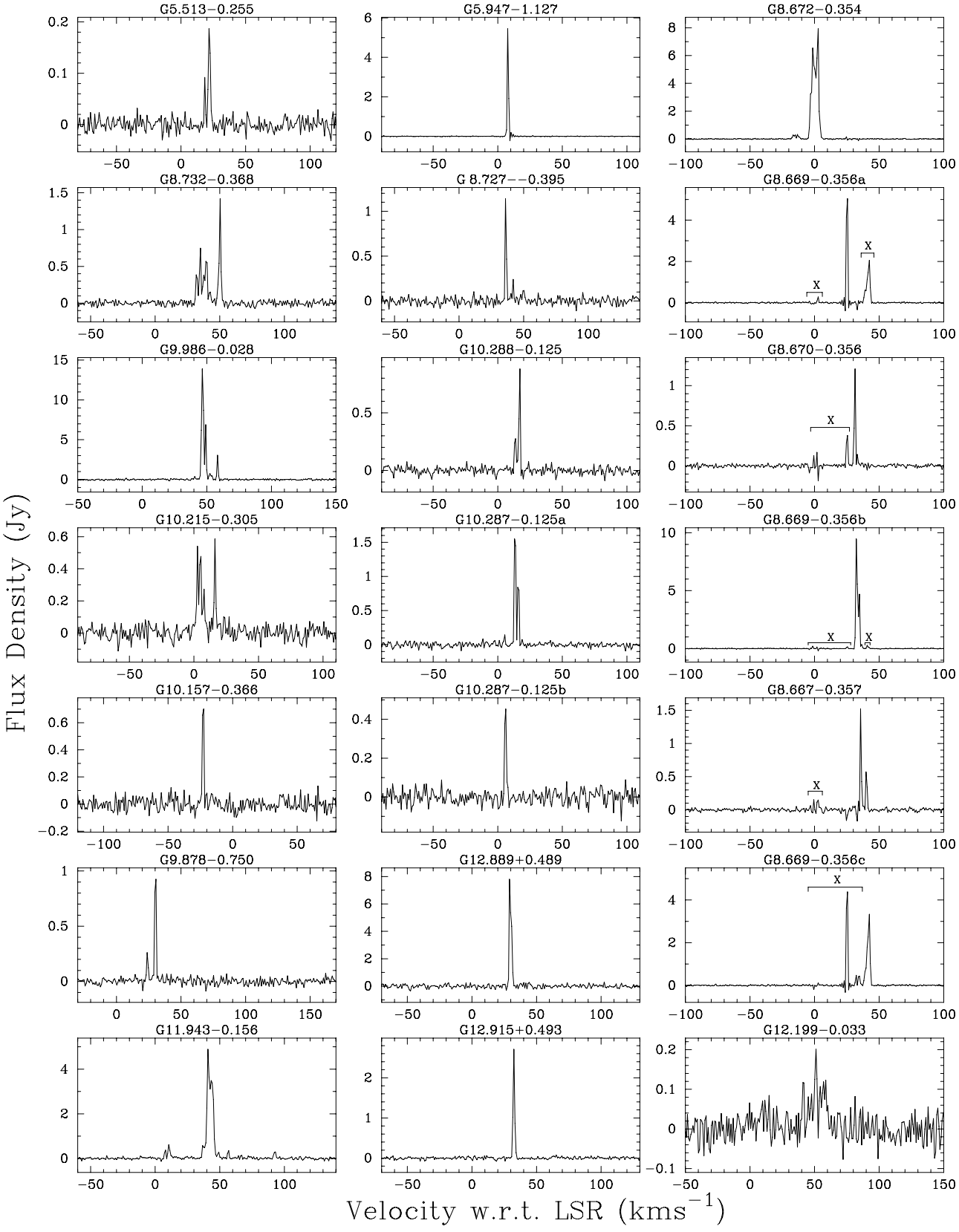

Figure 1 – *continued*

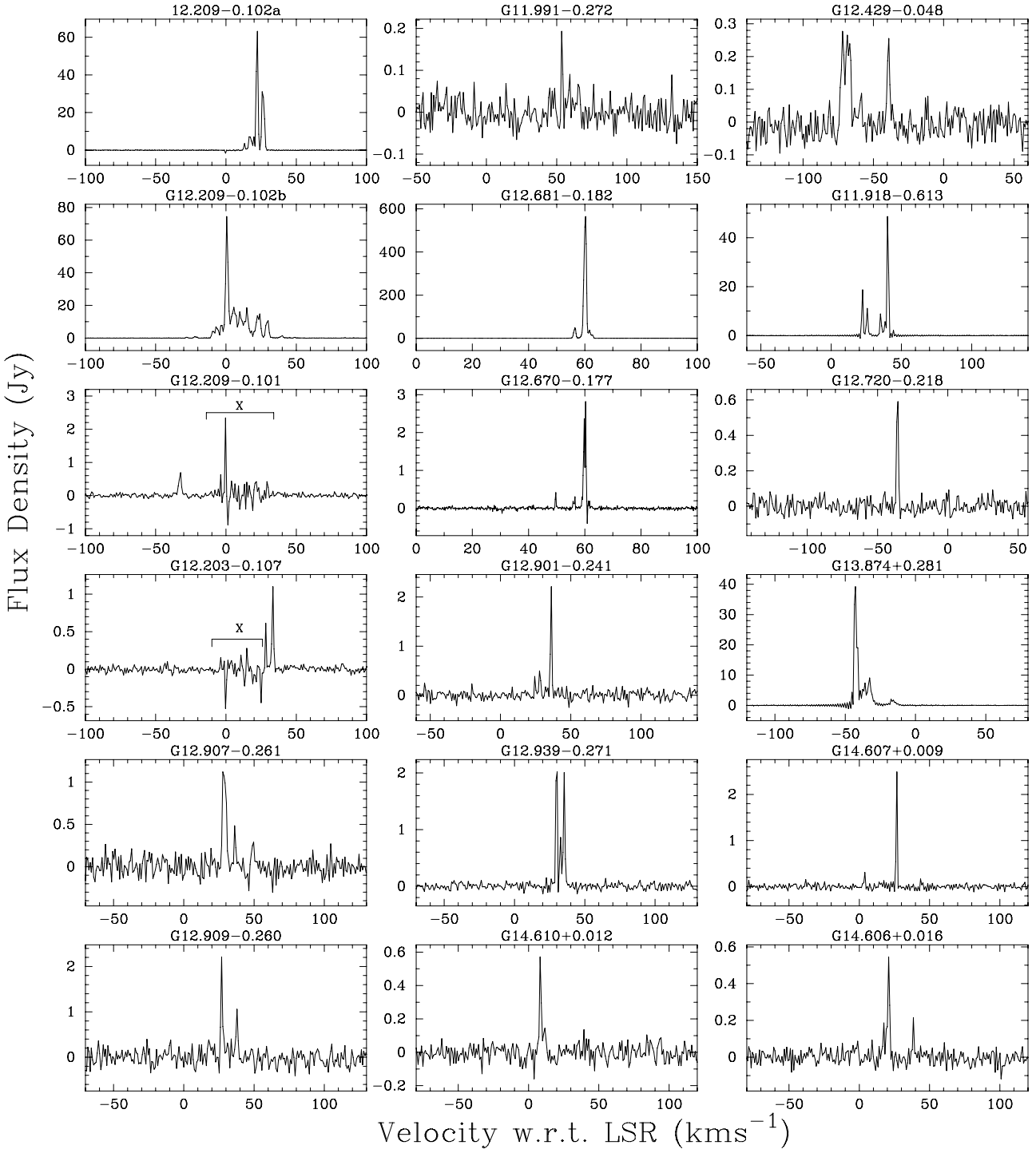

Figure 1 – *continued*

G 301.136−0.226. As noted in Breen et al. (2010b), emission from this source is significantly spread. In the observations carried out in 2008 July, we observe individual maser components spread over almost 5 arcsec. An OH maser is located within the spread of the water maser emission (Caswell 1998).

G 305.362+0.150. During the observations in 2008 August, we detected a moderately strong water maser exhibiting one main spectral feature. In 2004 (presented in Breen et al. 2010b) an additional, broader feature of more than 100 Jy was also detected and has disappeared intervening interval.

G 0.546−0.851b. This water maser falls within a cluster of three distinct water maser sites and has a velocity range that exceeds 170 km s^{-1}. The emission extends almost symmetrically about the peak water maser emission.

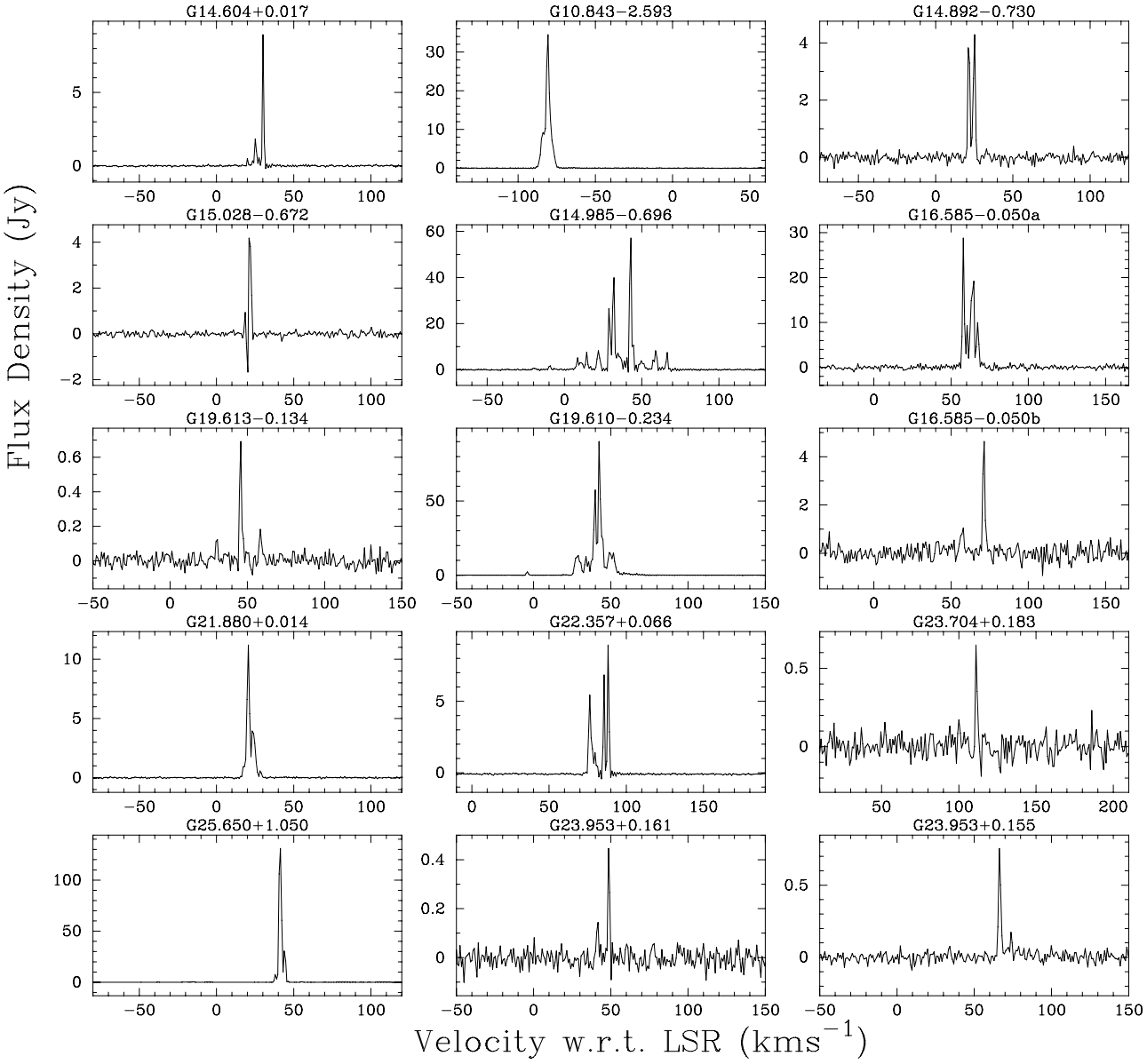

Figure 1 – *continued*

G 5.513−0.255. Like G 291.284−0.716, this water masers lies unusually close to the edge of the 1.2-mm dust clump emission that was observed by Hill et al. (2005). No other similarities between the sources are evident. This source is very weak and shows emission close to the likely systemic velocity of the region, while G 291.284−0.716 is very strong and is a dominant blueshifted source.

G 8.727−0.395. This water maser is clearly projected against 1.2-mm dust continuum emission on inspection of the corresponding dust map of Hill et al. (2005), although no dust clump is reported at this position. It is likely that this source was omitted from the catalogue of Hill et al. (2005) in error.

G 10.473+0.027 and G 10.480+0.034. The observations presented in Table 2 have been taken from Breen et al. (2010b). Both of the sources were detected in observations carried out in 2003, but G 10.480+0.034 had fallen below the detection limits in 2004 (<0.2 Jy).

G 11.903−0.142. The observations presented in Table 2 have been taken from the observations carried out in Breen et al. (2010b), and similarly to G 10.480+0.034, this water maser was detected in 2003, but by 2004 the emission had fallen below our detection limits. Since the emission detected in 2003 had a peak flux density of 0.3 Jy, this is not surprising.

G 12.209−0.101, G 12.429−0.048, G 12.720−0.218 and G 13.874+0.281. These four well-separated water maser sources all exhibit water maser emission at only negative velocities. From the velocities of nearby methanol masers, systemic velocities in this region of the sky would be expected to be between 20 and 60 km s^{-1}. Therefore, these sources are all potential candidates for the class of sources that are dominated by blueshifted emission.

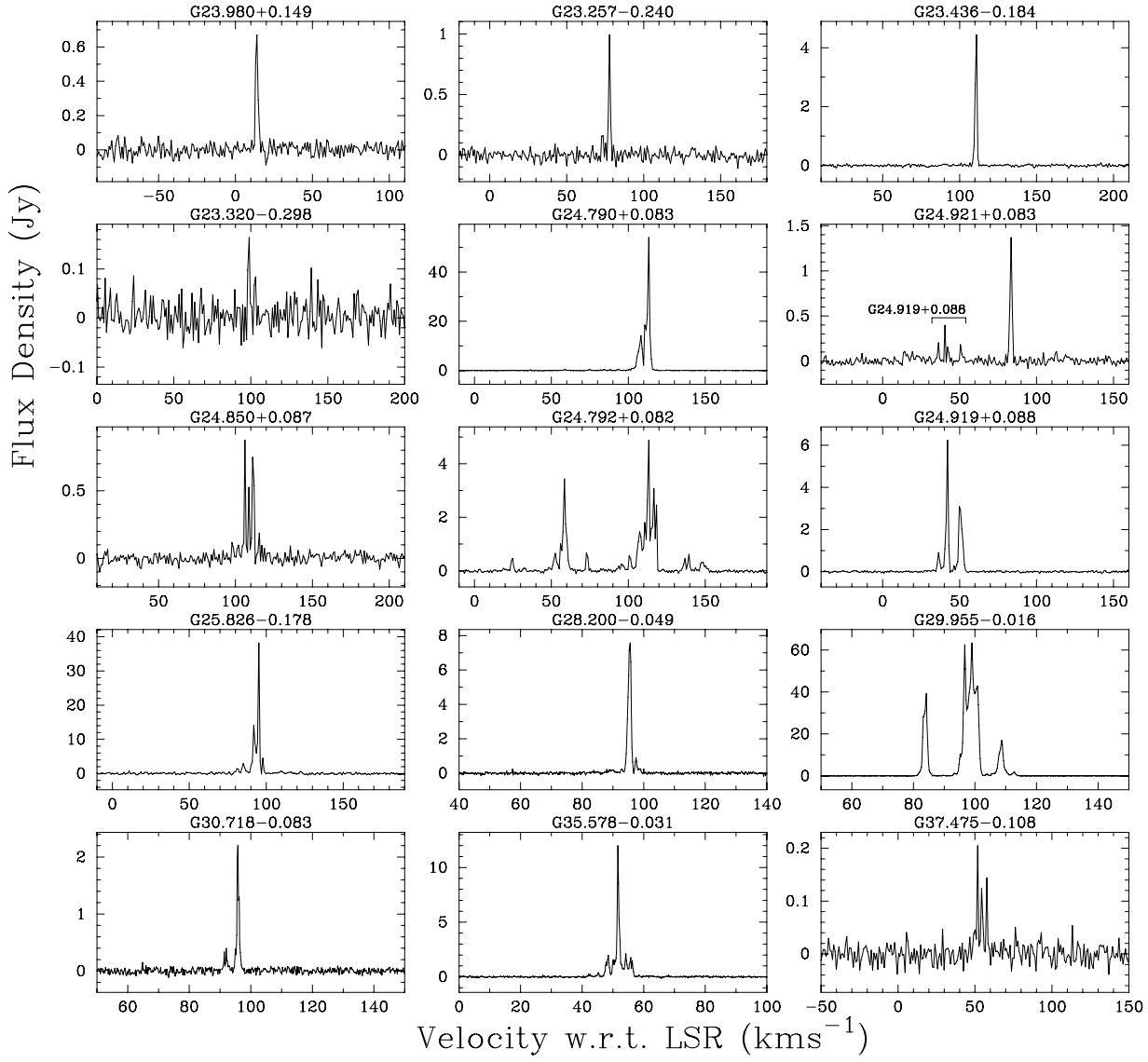

Figure 1 – *continued*

3.2 Water masers with no apparent associated dust continuum emission

In addition to the water maser sources presented in Table 2 and Fig. 1, we detect several other sources which are of special interest. While an exhaustive attempt to search for water maser emission beyond the boundaries of the 1.2-mm dust clumps was not made, here we list the additional water maser sources that were identified.

Interestingly, we find four water maser sources that appear not to be associated with any 1.2-mm dust clump emission and these are presented in Table 3 and Fig. 2. Hill et al. (2005) detected 1.2-mm dust clump emission in the fields of all of the target 6.7-GHz methanol masers and UCHII regions, but for 20 of the methanol masers and nine of the UCHII regions there is no spatially coincident dust continuum emission. Investigation by Hill et al. (2005) showed that these sources appeared to be no different to those where 1.2-mm dust continuum was detected. Since the presence of 1.2-mm dust clump emission indicates the presence of cold, deeply embedded sources, two of the possible explanations put forward by Hill et al. (2005) are that these sources are more evolved and hence no longer in the cold-core phase or, perhaps, they are less massive.

We have investigated possible mid-infrared counterparts for these four sources by comparing their locations with products from the Galactic Legacy Infrared Mid-Plane Survey Extraordinaire (GLIMPSE) survey. All are projected against regions of extended infrared emission, and two sources (G 19.612−0.120 and G 23.455−0.201) are coincident to within 1 arcsec of a GLIMPSE point source. Interestingly, the two sources with associated point sources are also associated with methanol masers. This suggests that these two sources may be located at the far distance and consequently were not detected in 1.2-mm dust continuum due to sensitivity limitations. The nature of the other two sources is more confusing and certainly warrants future investigation.

Unlike 6.7-GHz methanol masers, water masers have been detected towards both evolved and low-mass stars. Their presence in locations devoid of 1.2-mm dust continuum emission is therefore much more easily accounted for than methanol masers. Comments on each of these four water masers are given below.

Table 3. Four water maser sources detected in the target fields that are not coincident with any detected 1.2-mm dust clump emission. Columns (1)–(7) give the water maser source name, water maser right ascension, declination, peak flux density (Jy), velocity of the water maser peak emission (km s^{-1}), velocity range (km s^{-1}) and the integrated flux density of the water maser emission (Jy km s^{-1}), respectively.

Name (l, b) (degrees)	RA (J2000) ($^{h\,m\,s}$)	Dec. (J2000) ($^{\circ}\,'\,''$)	Sp (Jy)	Vp (km s^{-1})	Vr (km s^{-1})	Int (Jy km s^{-1})
G 305.248+0.195	13 11 34.84	−62 35 11.0	7	−93	−95, −92	9
G 19.612−0.120	18 27 13.55	−11 53 14.7	1.2	58	57, 60	1.6
G 23.397−0.219	18 34 42.32	−08 34 43.3	7	102	97, 106	14
G 23.455−0.201	18 34 44.89	−08 31 07.4	3.1	82	57, 84	17

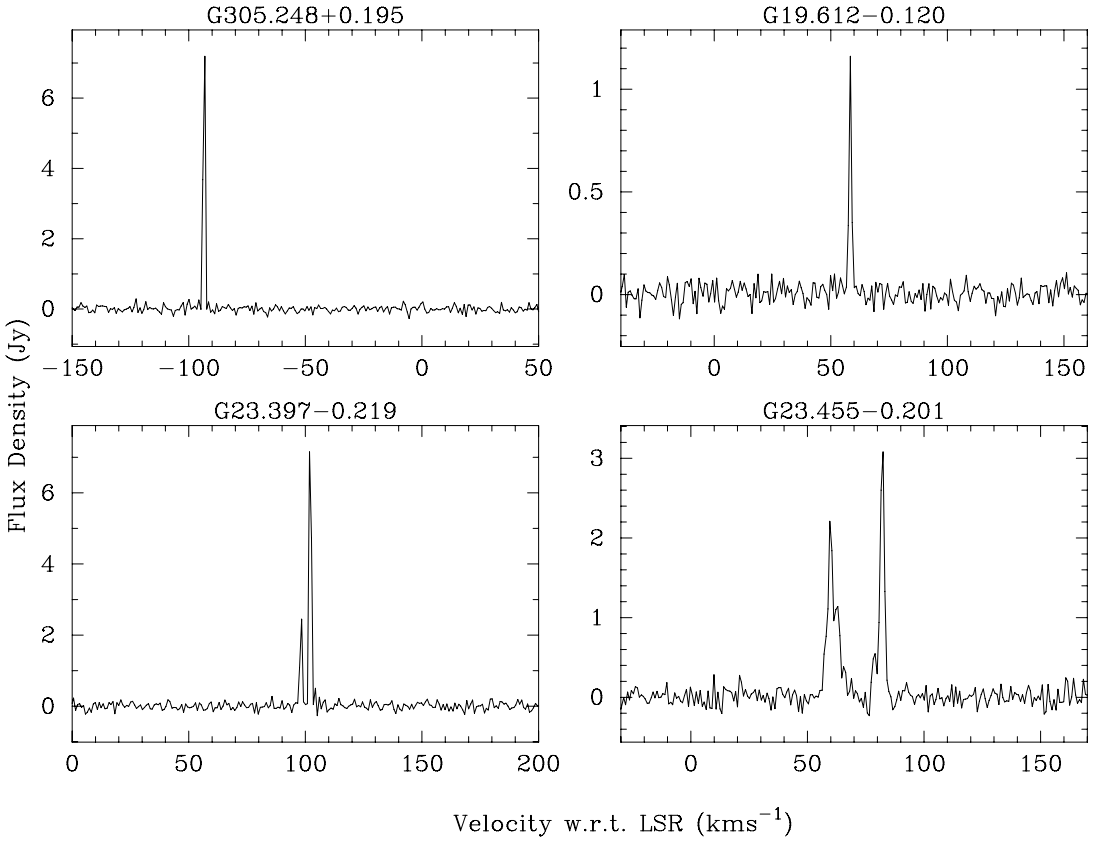

Figure 2. Water maser sources with no associated 1.2-mm dust clump emission, detected within the target fields.

G 305.248+0.195. This water maser is separated from the boundary of the nearest dust clump by more than an arcmin.

This source falls beyond the latitude range completely searched for the presence of water maser emission by Caswell & Breen (2010) which was focused on a region bounded by a longitude range of 305.°0–306.°26 and ±0.°15 latitude. A total of 23 water maser sources were detected in this portion of the Galactic plane. Analysis of the masers found in this area, along with another region (longitude range of 311.°0–312.°18 and ±0.°15 latitude) showed a surprising preponderance of sources with highly blueshifted emission. Investigation by Caswell & Breen (2010) led to a suggestion that these water masers represent a population of sources that are tracing a very early evolutionary stage, perhaps preceding the stage where 6.7-GHz methanol masers are seen.

Interestingly, G 305.248+0.195 only shows emission at a blueshifted velocity of −95 km s^{-1} (nearby methanol masers detected in the Methanol Multibeam Survey exhibit peak velocities between −40 and −30 km s^{-1}), and therefore adds to the already high number of blueshifted sources in this region of the Galactic plane. However, the interpretation that such sources may be very young directly contradicts one of the suggestions given by Hill et al. (2005) as to why some sources are devoid of 1.2-mm dust continuum emission – that they are more evolved. Alternatively, it is possible that this water maser is associated with a low-mass object, although a high-velocity feature >50 km s^{-1} from the systemic velocity of the region would be unusual for a low-mass star.

G 19.612−0.120. This water maser is coincident with one of the methanol masers from Walsh et al. (1998) that was targeted by Hill et al. (2005), but is also offset from the boundary of the nearest dust clump by about an arcminute. Green et al. (2010) present evidence suggesting that this methanol maser is located at

the far distance, which would limit the sensitivity of the 1.2-mm dust continuum observations, but not to the extent that no detection of dust continuum emission would be expected.

G 23.397−0.219 and G 23.455−0.201. Both of these water masers fall within the one dust continuum emission map, but neither are directly associated with any detectable dust continuum emission. The first source is apparently solitary (i.e. without any associated UCHII region or 6.7-GHz methanol maser emission), but the second source appears to be coincident with an UCHII region reported by Walsh et al. (1998).

4 DISCUSSION

4.1 Detection statistics

Altogether, we find water maser emission towards 128 of the 294 1.2-mm dust clumps, equating to a detection rate of 44 per cent. Investigation of the detection rate of water masers towards 1.2-mm dust clumps shows some variation with Galactic longitude. The water maser detection rate towards dust clumps located between longitudes of 213° and 333° is 55 per cent (51 of 93), compared with 38 per cent (77 of 201) for the longitude range 0°–38°. Although not covering exactly the same longitude ranges, it is curious to note that the detection rates of 12.2-GHz methanol masers in the longitude range 270°–305° were significantly lower than in other parts of the Galaxy (Breen et al. 2011). If it were the relative distances that were affecting our detection rates, then, if anything, we would expect to have a lower detection rate in the 213°–333° longitude region as we would expect relatively more dust clump detections in these regions. Since our maser observations are of a high sensitivity, we would expect a minimal detection rate dependence on distance. Caswell & Breen (2010) and Caswell et al. (2011) completed systematic searches for water masers within three regions of the Galactic plane. They show that there is a large difference in the water maser population densities within these regions, suggesting that local factors have an effect on the detection statistics. It is therefore possible that there are broader localized effects contributing to our detection statistics here. This warrants further investigation, but is beyond the scope of this paper.

4.2 Characteristics of the detected water masers

4.2.1 Velocity ranges and flux densities of the complete sample

The average velocity range of the 165 water masers is 26 km s^{-1} and they have a median velocity range of 13 km s^{-1}. In comparison, the average velocity range of the 379 water masers detected by Breen et al. (2010b) is 29 km s^{-1} and they have a median velocity range of 15 km s^{-1}. While these numbers are quite similar, it is intriguing that velocity ranges of the sources that are potentially biased towards more evolved sources are, in general, larger than those detected towards the sample of dust clumps. Breen et al. (2010b) chiefly targeted their observations towards OH masers. Breen et al. (2011) present evidence that suggests that both the 6.7- and 12.2-GHz methanol maser sources show an increase in velocity range as the sources evolve. Although complicated by the presence of high-velocity features, we have carried out a similar analysis on the water masers in Section 4.2.2.

Further evidence that these water masers are less biased towards more evolved sources lies in the average and median flux density of the detected sources. Breen et al. (2010b) present evidence that the water masers increase in flux density as the sources evolve. The average flux density of the water masers detected towards the dust clump sample is 39 Jy and they have a median of 4 Jy which are both lower than the average (57 Jy) and median (5 Jy) flux density of the sources presented in Breen et al. (2010b). This suggests that in the dust clump sample, we have detected water masers over a broader range of evolutionary stages.

4.2.2 Association with other maser species and radio continuum

Hill et al. (2005) determined associations between their 1.2-mm dust clump sources and the 6.7-GHz methanol masers and UCHII regions (detected at 8 GHz) towards which their observations were targeted. We have made an investigation of the number of dust clumps, with and without associated water masers, that Hill et al. (2005) have designated as being (i) 'mm-only' cores (i.e. sources without associated radio continuum emission or 6.7-GHz methanol masers), (ii) associated with 6.7-GHz methanol masers, (iii) associated with both 6.7-GHz methanol masers and radio continuum, and finally (iv) associated with only radio continuum. In all of our statistical analysis, 293 of the 294 targets for water masers have been included (omitting a single source which is missing values for some dust clump properties).

Table 4 shows a summary of the categories of dust clumps where we detect the water masers, as well as the water maser detection rate in each category. We find an overall water maser detection rate of 44 per cent towards the targeted dust clumps, and this number falls to 23 per cent for the 'mm-only' dust clump sources. The highest water maser detection rates are towards those dust clump sources that exhibit methanol maser emission, closely followed by those dust clumps showing only radio continuum emission. It can be seen that there are many more dust clump sources showing only water masers (41) than those showing only methanol masers (13). While some fraction of these 1.2-mm sources that show only methanol masers are likely to have associated water masers that were below our detection limits at the time of observation, it seems unlikely that this could be the case for all of them (by considering the statistics of detectability for the two epochs of water maser observations presented in Breen et al. 2010b). However, these sources will provide interesting targets for further water maser observations. Hill

Table 4. Water maser detection rates in each dust clump category (from Hill et al. 2005): 'mm-only' (those sources showing no associated methanol maser or radio continuum emission), associated methanol masers (meth), associated with both methanol masers and radio continuum associations (meth+cont), and associated continuum (cont). These numbers have been presented in two categories: those dust clumps with no detectable water maser emission and those where we have detected water masers. The fourth column shows the water maser detection rate (per cent) in each of the categories.

	No water	Water	Detection rate (per cent)
'mm-only'	137	41	23
meth	13	48	79
meth+cont	5	25	83
cont	10	14	58
Total	165	128	44

Table 5. The average and median flux densities, and velocity ranges of all of the detected water masers. Water maser sources have been broken up into several categories, and are as for Table 4, with the addition of 'all sources' which shows the values for the entire sample.

Water classification	Average flux density (Jy)	Median flux density (Jy)	Average vel range ($km\,s^{-1}$)	Median vel range ($km\,s^{-1}$)
all sources	39	4.4	26	13
'mm-only'	2	1.5	19	8
meth	44	9	28	19
meth+cont	107	18.5	42	23
cont	9	1	26	17

et al. (2005) suggests that their 'mm-only' cores may represent an earlier evolutionary phase than those sources showing methanol maser emission. If this is the case, these numbers certainly imply that water masers can be present even earlier than methanol masers. A supporting argument for water masers having a longer lifetime than that of methanol masers is that water molecules are both more easily created and more robust than methanol, which is consistent with our interpretation.

An alternative explanation for the higher number of dust sources showing only water masers (than those showing only methanol masers) is that a number of these additional water masers are associated with lower mass objects. Comparing the dust clump properties in each of the association categories offers no evidence for there being any systematic differences between the groups which may result if a large number of these sources were lower mass objects.

We have investigated the water maser characteristics in each of the dust clump association categories. Table 5 presents the average and median values of both the water maser peak flux density and the velocity range. Like the methanol masers presented by Breen et al. (2011), we find that there is a general gradient which trends from lower values of both flux density and velocity range for the (probably) younger sources to higher values for the more evolved sources. This trend progresses through the categories as follows: those associated with 'mm-only' sources to those with methanol masers, and then to those with methanol masers and radio continuum (Hill et al. 2005; Breen et al. 2010a). The exception to this trend is the last stage, where only radio continuum is seen.

If the numbers presented in Table 5 are representative of the larger population of water masers, then they imply that, while the water masers increase in flux density and velocity range as the sources evolve, towards the end of their lifetime this trend 'turns over' and they steadily decrease in both flux density and velocity range, presumably decreasing until the maser emission ceases. This is contrary to that seen in the case of methanol masers (Breen et al. 2011), which seem not to experience any downward trend, implying that they switch off much more abruptly.

Comparing the luminosities of the water masers (calculated using the near distances presented in Hill et al. 2005) with the velocity ranges of the water maser sources similarly shows an increase in both luminosity and velocity range through the different association categories from least to most evolved. However, there is a significant overlap between the values within each association category. A high level of scatter is expected when considering water masers, since a number of sources show high-velocity features, and it is not clear that these are restricted to a certain evolutionary stage. Also, the sources that are associated with only 8-GHz radio continuum are scattered throughout the range of values that are associated with the sources in other categories, but none has large values of luminosity,

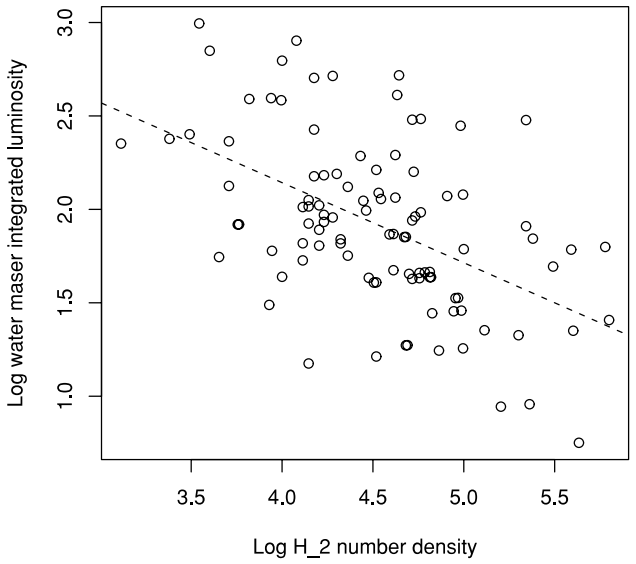

Figure 3. Log water maser integrated luminosity ($Jy\,km\,s^{-1}\,kpc^2$) versus log of the H_2 number density (cm^{-3}) of the associated 1.2-mm dust clump. The dashed line shows the line of best fit (which has a slope of −0.43[0.07], an intercept of 3.86[0.33] and a correlation coefficient of 0.50).

and very few have large velocity ranges. These findings are consistent with those conclusions drawn from the average values that are presented in Table 5 where peak flux densities are considered.

4.2.3 Comparison between water maser luminosity and 1.2-mm dust clump H_2 number density

Breen et al. (2010a) shows that the H_2 number density of the 1.2-mm dust clumps decreases as the sources evolve. However, as noted by Breen et al. (2010a), the apparent change in density might be a consequence of the constant temperature assumption applied by Hill et al. (2005) in their calculations and consequently the difference in densities might instead represent an increase in temperature. In either case, the changes to the physical properties of the source are consistent with evolution.

In Fig. 3 we present the log of the integrated water maser luminosity versus the log H_2 number densities of the associated 1.2-mm dust clumps. This plot show a slope that is consistent with the findings of Breen et al. (2010a) and those previously presented in this section – that the more luminous water masers are more evolved and that these are associated with the less dense 1.2-mm dust clumps and vice versa. Table 6 compares the computed slopes and intercepts of the line of best fit of the log luminosity 6.7- and 12.2-GHz methanol masers, along with the water masers versus the H_2 number densities of the associated clumps.

Table 6. Slopes and intercepts of the line of best fit of log integrated maser luminosity versus log of the H_2 number densities of the 1.2-mm dust clumps. Values for 6.7- and 12.2-GHz methanol masers are listed for comparison with the water maser values. Errors are presented in square brackets and follow the estimates of each value.

Maser species	Slope	Intercept	Reference
6.7 GHz	−0.72[0.25]	5.53[1.17]	Breen et al. (2011)
12.2 GHz	−0.56[0.28]	4.16[1.23]	Breen et al. (2010a)
Water	−0.43[0.07]	3.86[0.33]	This paper

Inspection of the values listed in this table show first (as previously stated) that the 6.7-GHz methanol masers increase in flux density more rapidly as they evolve than the associated 12.2-GHz sources and, as shown by the larger intercept, are generally stronger than the 12.2-GHz sources. Interestingly, the values associated with the water maser sources imply that the water masers also increase in flux density less rapidly than the 6.7-GHz methanol masers as they evolve and are also weaker in general at a given H_2 number density (than the sample of 6.7-GHz methanol masers). However, it is difficult to determine which of the maser species are present at the earliest evolutionary stage of high-mass star formation and therefore which species shows stronger emission at a given evolutionary stage.

4.2.4 Water maser variability

Water masers are known to exhibit extreme variability over relatively short time-scales (e.g. Felli et al. 2007). The water maser observations presented in Breen et al. (2010b) were completed, in many cases, twice with the observation epochs separated by ∼10 months. Additionally, Caswell & Breen (2010) carried out a double-epoch search for water maser emission of two small regions of the Galactic plane. Since the observations presented here were completed only once, we cannot directly determine the level which maser variability has affected our results. Instead, we derive predictions about the completeness of these observations by comparing this sample with the findings of Breen et al. (2010b) and Caswell & Breen (2010).

Breen et al. (2010b) find that 17 per cent of the 253 water maser sources that were observed at two epochs were only detectable at one of these epochs. Caswell & Breen (2010) found similarly that 16 per cent of the 32 sources that they detected in their double-epoch complete searches were detectable only once. If we simply apply the larger percentage (i.e. 17 per cent) to our current sample, it might be expected that ∼34 additional water maser sources would be detected if a second epoch of observations were conducted towards the target 1.2-mm dust clumps. Since we detect 165 water masers towards 128 1.2-mm dust clumps, we would perhaps expect that these additional sources would be detected towards a further 26 1.2-mm dust clumps.

However, the situation is a little more complex than this. It is not clear if the role of variability would result in many more dust clumps being recognized as being associated with water masers, or alternatively that different water maser sources would be detected at different epochs towards the same dust clump. It is likely that both would be true, that is, that some number of water masers would be detected towards additional 1.2-mm dust clumps and that some additional/different water masers would be detected towards 1.2-mm dust clumps where we have detected water masers.

4.3 Location of the water masers in the 1.2-mm dust clumps

Analysis of the locations of the water masers with respect to the 1.2-mm dust clump peak, as reported by Hill et al. (2005), shows that there is excellent correspondence between their locations. The 1.2-mm dust continuum maps of Hill et al. (2005) have 8-arcsec pixels, and the listed peak positions are just the central position of the peak pixel. On average, we find that the separation between the water maser positions and the associated dust clump peak is 13 arcsec and that the median separation is 8 arcsec. It is therefore likely that, in the majority of cases, the water masers are very closely associated with the peak 1.2-mm dust clump emission.

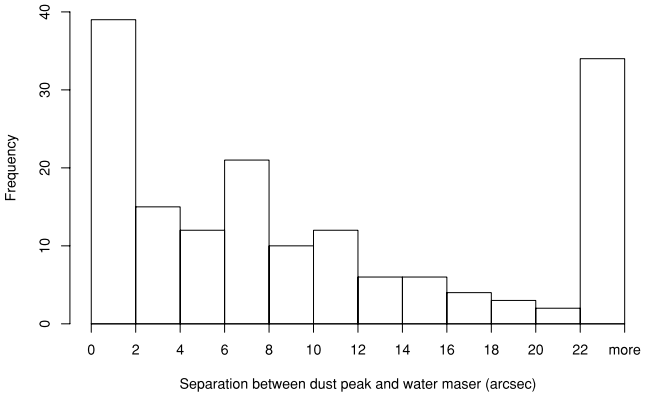

Figure 4. Histogram of the angular separation between the reported 1.2-mm dust clump peak and the position of the water maser sources.

Fig. 4 shows a histogram of the separations between the dust clump peak and the detected water masers. All water masers that were separated by more than ∼30 arcsec from the dust clump peak were further investigated by comparing the reported dust clump peak position with the dust maps presented in figure A1 of Hill et al. (2005) and the water maser positions. We find in just over half of these cases (11 of 19) that there is an obvious error in the reported dust clump position which has led to an apparently large separation from the water maser position. In the worst examples, the reported dust clump peak is located beyond the boundary of the respective clump. Even though Hill et al. (2005) publish images of their 1.2-mm dust clumps, the resolution (and contrast) is insufficient to enable us to determine better positions independently. Given the obvious problems with some number of the dust clump peak positions which erroneously result in some of the most extreme separations between the peak of the clump and the associated water maser, it is likely that the actual average and median separations between the peak of the dust clumps and the associated water masers would be even smaller, perhaps comparable to the pixel size.

We have compared the locations of the water masers with respect to the location of their associated dust clump peak and the peak flux density of the maser sources. It is evident that very few of the water masers that are truly significantly offset from the peak of the dust clumps have flux densities that are greater than a few Jy. The possible corollary, that most of the water masers that are located far from the dust clump peak are relatively weak, needs further investigation.

4.4 Assessing the current model of water maser presence in 1.2-mm dust clumps

Breen et al. (2007) created a model for water maser presence towards 1.2-mm dust clumps which was derived from observations of the 1.2-mm dust continuum emission (Mookerjea et al. 2004) and water maser observations that they completed within the G333 GMC. By determining which 1.2-mm dust clumps were associated with water masers as well as those that were devoid of water maser emission, Breen et al. (2007) fitted a binomial generalized linear model to the maser presence/absence data, using the 1.2-mm dust clump properties as predictors. They found that the simplest model with the greatest predictive properties was based only on dust clump radius.

We have used the model derived by Breen et al. (2007) to calculate the probability of water maser detection for each of the dust clumps presented in Hill et al. (2005) that have dust clump

radius measurements. For a number of dust sources presented in Hill et al. (2005), there is a near–far distance ambiguity. In these cases, we have assumed the near distance for consistency with analysis completed by Breen et al. (2010a). However, we note that in this instance this assumption might be particularly hazardous, since the predictive model relates only to 1.2-mm dust clump radius which is highly influenced by the adopted distance measurement.

Using the model for water maser presence associated with 1.2-mm dust clumps, it was determined that only 58 of the 294 dust clumps considered in this analysis had a probability of 0.01 or greater of having an associated water maser. Probabilities for individual dust clumps are presented in Table 2. Comparison between the calculated probability of water maser and the actual detections shows that the model described in Breen et al. (2007) is promising. The average probability of water maser presence in the 128 1.2-mm dust clumps where water masers are detected is 0.10, and has a median value of 0.000 81. In comparison, for the dust sources where we detect no water maser emission, the average probability of water maser presence is 0.027 and has a median value of 0.000 26. An alternative description of these statistics is that, of the 27 1.2-mm dust clumps which had a calculated probability of $\geq$0.1, 20 yielded water maser detections. If the considered probability is lowered to $\geq$0.01, then the number of predicted clumps is increased to 58, and the number of clumps with detections is 39. It is therefore clear that the model is picking up a high detection rate for the sources with high calculated probabilities; however, given that we detect water masers towards 128 dust clumps, it is also clear that the model is failing to return high probabilities of water maser presence in around two-thirds of the clumps with detections.

Given that the original model was derived from a sample of water masers that were detected in a complete search with a relatively poor sensitivity limit ($\geq$5 Jy), the obvious property to investigate is the relative flux density of the detected water masers. It might be expected that there would be a trend whereby the water maser detections towards the 1.2-mm dust clumps with high association probabilities have higher flux densities, given the nature of the data on which the model was derived. The average flux density of the water maser sources detected towards dust clumps with a probability of 0.01 or higher (58 water maser sources) is 48 Jy, and these sources have a median flux density of 6 Jy. In comparison, the average flux densities of the water masers detected towards clumps with a lower calculated probability is 33 Jy, with a median flux density of 3.5 Jy. It is possible, therefore, that the current model is biased towards predicting correctly the presence of the stronger sources. However, more likely is that the sources with very low probabilities are dominated by far-distance sources which accounts for the lower average flux density (which would also mean that their probabilities have been under estimated).

Another obvious factor to consider is the high degree of dependence on distance measurements. Since the original model was derived from sources located within the one GMC with a well-constrained distance measurement, the poorly determined distances towards most star formation regions did not affect the generation of this model. The model for water maser presence associated with dust clumps uses only the radius of the dust clump in order to calculate the probability. As previously discussed, we have assumed the near distance reported by Hill et al. (2005) for sources with distance ambiguities. It is clear that this is an unreliable assumption, especially since our search is of high sensitivity which reduces the likelihood of any significant detection dependence on distance. It would be expected that the split of near and far-distance allocations should be approximately even (or maybe even favour the far distances due to the large volume). Inspection of the characteristics of some of the dust clump sources that have low calculated probabilities, yet have associated water masers, shows that if the far distance was used, then the calculated probability would be high (in many cases $>$0.3). The increase in radius that results in a change from near-to-far distance does not result in a high probability in water maser presence in all of the dust clump sample, especially those with no detected associated water masers.

If our assertion, that the poorly constrained distance measurements are adversely affecting the predictive capabilities of the model, is correct, then the distribution of the clump properties should support this. If, for example, we inspect the peak flux density of the 1.2-mm dust clumps with associated water masers and calculated probabilities of $>$0.01, then they should not be any different from the sample of 1.2-mm dust clumps with associated water masers and calculated probabilities of $<$0.01. However, they are in fact different. The average peak flux density of the clumps with calculated probabilities of $>$0.01 (and have associated water masers) is 2.8 Jy beam^{-1}, whereas the average of those clumps with lower than expected calculated probabilities ($<$0.01) is 1.4 Jy beam^{-1}. Again, the most likely explanation for this is that a number of the 1.2-mm dust clumps which have low calculated probabilities, but yet have an associated water maser, are located at the far distance. This means that the seeming downfall of the model to allocate high probabilities to a number of the 1.2-mm dust clumps where we detect water masers may be eradicated if accurate distance measurements were obtained.

4.5 Fitting binomial general linear models to the new water maser and 1.2-mm dust clump data

While the current model for water maser presence in 1.2-mm dust clumps is promising, we have repeated the analysis carried out by Breen et al. (2007) with the much larger sample presented here. However, two important considerations are, first, the adoption of the near-distance measurements for the sources with distance ambiguities and, secondly, that the 1.2-mm dust clumps in this sample were not detected in a systematic manner (unlike the observations of Mookerjea et al. 2004 used in Breen et al. 2007), although given the high number of additional 1.2-mm dust sources found within the fields of the target sources this is probably not detrimental to the analysis.

We have fitted a binomial generalized linear model to the water maser presence/absence data, using the 1.2-mm dust clump properties as predictors. For a more detailed description of this analysis method, see Breen et al. (2007). All but one of the targeted 1.2-mm dust clumps were included in this analysis. The source that has been excluded is G 6.60−0.08 as Hill et al. (2005) suggest that the derived mass of this source is uncharacteristic of high-mass star formation regions. For each of the 1.2-mm dust clumps, all of the derived clump properties were tested: the integrated flux density (Jy), peak flux density (Jy beam^{-1}), source FWHM (arcsec), distance (kpc), mass ($M_{\odot}$), radius (pc) and H_2 number density (cm^{-3}). In the following sections we consider *p*-values of less than 0.05 to be statistically significant (i.e. the hypothesis that the single-term model provides no better fit than the null model consisting only of an intercept is rejected when the *p*-value is less than 0.05).

First, all dust clump properties were tested to see if individually they could give an indication of the likelihood of associated water maser presence. This was done by fitting a single-term addition binomial model to each property (or 'predictor') and showed an increasing probability of the presence of water masers associated with

Table 7. Analysis of deviance table for the single-term models (using the 1.2-mm dust clump properties from Hill et al. 2005), showing the deviance and the AIC together with the associated likelihood ratio statistic and *p*-value for the test of the hypothesis that the stated single model provides no better fit than the null model consisting only of an intercept.

Predictor	Deviance	AIC	LRT	*p*-value
None	399.84	401.84		
Integ	341.81	345.81	58.02	2.590e−14
Peak	332.98	336.98	66.85	2.923e−16
FWHM	354.23	358.23	45.61	1.445e−11
Dist	398.65	402.65	1.19	0.2761
Mass	366.41	370.41	33.43	7.391e−09
Radius	379.44	383.44	20.40	6.299e−06
Density	399.66	403.66	0.18	0.6697

increasing values of dust clump integrated flux density, peak flux density, FWHM, mass and radius (shown in Table 7). This result is similar to that found when investigating methanol masers (Breen et al. 2010a), and means that any one of these dust clump properties can give an indication of the likelihood of finding an associated water maser. Box plots of each of the dust clump properties broken up into the categories of 'n' and 'y', referring to those clumps with no associated water maser and those with an associated water maser, respectively, are presented in Fig. 5. These box plots show graphically the same information as the results of the single-term additions, that is, lower values of the dust clump properties, integrated and peak flux density, FWHM, mass and radius, are associated with the 1.2-mm dust clump sources with no associated water maser emission, compared to those associated with water maser emission.

After determining the predictive capabilities of individual dust clump properties, stepwise model selection was used to create the simplest model with the greatest predictive power. This method considers all of the dust clump properties and tries to maximize the predictive properties while trying to minimize the number of terms (and therefore dust clump properties). The resultant model contains only two dust clump properties: peak flux density and FWHM. The estimated regression relation is

$$\log \frac{p_i}{1-p_i} = -1.564 + 0.995 x_{\rm Peak} + 0.012 x_{\rm FWHM},$$

where $x_{\rm Peak}$ is the peak flux density, $x_{\rm FWHM}$ is the source FWHM and p_i is the probability of finding a water maser towards the ith 1.2-mm dust clump. The regression summary of this model is shown in Table 8. In contrast to the previous data set where a model based on dust clump radius (pc) was found to be best, the current data set uses dust clump peak flux density and FWHM (arcsec). As can be seen in Table 8, the dust clump peak flux density is the most influential term, indicated by the large standard error relative to the coefficient of the dust clump FWHM together with the large *p*-value.

The misclassification rates for this new model are somewhat promising when the probability threshold is set to 0.5, it correctly predicts half (63 of 127) of the dust clump sources with associated water masers, and it correctly predicts 144 of the 166 dust clumps with no associated water masers. It is easy to understand why such a model would fail on a high number of the dust clumps with associated water masers, since we know that these sources have higher peak flux densities on average; however, as can be seen in Fig. 5, there is a large overlap in the range of values of this property between those clumps with associated water masers and those without. This is consistent with a number of dust clumps with associated water masers having apparently low peak flux densities, since they are located at the far distance. Therefore, a peak flux density measurement that is scaled with reliable distance measurements (a pseudo-luminosity) may offer a promising model. Likewise, a reliable model may be derived from radius measurements that have correctly accounted for distances.

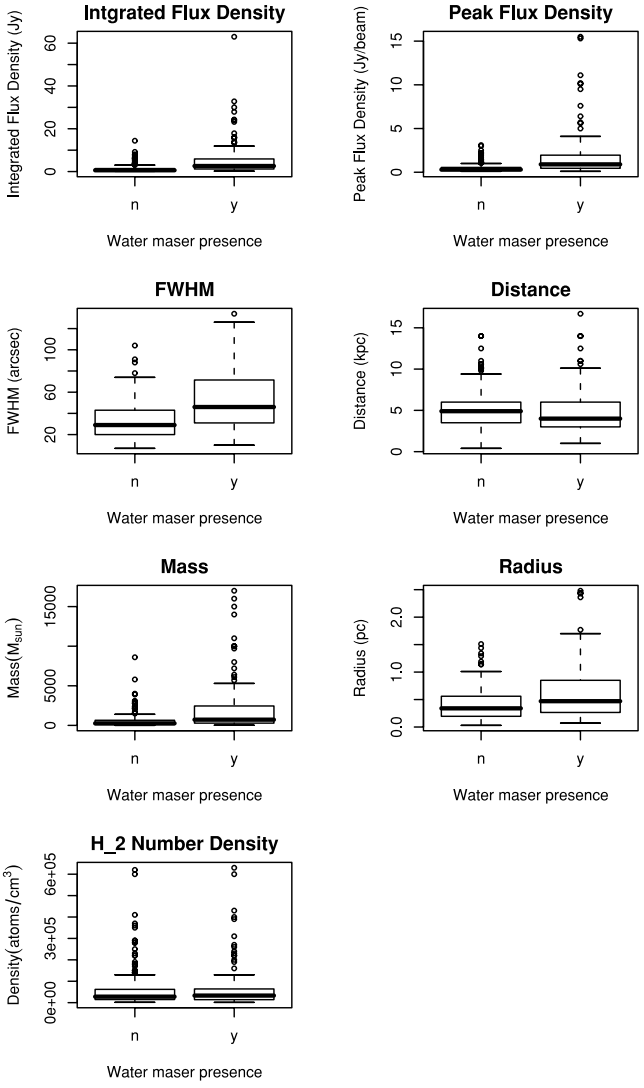

Figure 5. Box plots of the 1.2-mm dust clump properties split in the categories of yes and no, referring to the presence of water maser emission. There is a statistically significant difference between the two categories in the 1.2-mm dust clump integrated and peak flux density, mass, FWHM and radius. This information is the graphical display relating to the information in Table 7. Note that source G 23.960+0.137 has been removed from these plots, since it is more than twice as dense as all of the other sources shown on the plot and therefore is an extreme outlier.

4.5.1 A new model based on 1.2-mm dust clump radius

Since the model for water maser presence presented in Breen et al. (2007) uses only the dust clump radius to predict the probability of associated water maser presence, for comparison, a model using only dust clump radius has been produced from these new data. The resultant estimated regression relation is

$$\log \frac{p_i}{1-p_i} = -0.981 + 1.45 x_{\rm radius},$$

Table 8. Summary table for the Binomial regression model, showing for each predictor the estimated coefficient and the standardised z-value and p-value for the test of the hypothesis that $\beta_i = 0$.

Predictor	Estimate	Std. error	z-value	p-value
Intercept	−1.563 746	0.271 202	−5.766	8.12e−09
Peak	0.994 999	0.254 413	3.911	9.19e−05
FWHM	0.011 744	0.007 242	1.622	0.105

Table 9. Summary table for the Binomial regression model using only dust clump radius, showing the estimated coefficient and the standardised z-value and p-value for the test of the hypothesis that $\beta_i = 0$.

Predictor	Estimate	Std. error	z-value	p-value
Intercept	−0.9814	0.2101	−4.670	3.01e−06
Radius	1.4460	0.3544	4.081	4.49e−05

where $x_{\rm radius}$ is the radius of the 1.2-mm dust clump and p_i is the probability of finding a water maser towards the ith 1.2-mm dust clump. The regression summary of this model is shown in Table 9.

Since only one dust clump property is present in the regression relation, it is easy to determine the physical implications of the model. For example, if the probability of water maser presence is set to 0.5, the corresponding dust clump radius is 0.68 pc. This means that the model is saying that 1.2-mm dust clumps with a radius of 0.68 pc (or higher) have a probability of 0.5 (or higher) of having an associated water maser. In comparison, the model presented by Breen et al. (2007) predicts that 1.2-mm dust clumps with radii greater than 1.25 pc for the same probability threshold of 0.5 will have associated water masers. The model produced with the current data predicts that water masers are associated with much smaller dust clumps (about half the size, which is perhaps not surprising given that these observations are of much higher sensitivity), albeit relatively poorly. The misclassification rates from this new model are poor, particularly in determining which clumps will have associated water masers (which it gets wrong two-thirds of the time).

The poorly constrained distance measurements are therefore having a large effect on our ability to model the water maser presence within the 1.2-mm dust clumps. However, the higher accuracy of the models in predicting the sources without associated water masers may indicate that there is a population of sources that are significantly far from the properties of the clumps that exhibit water masers that not even a change from near to far distance would boost them to a high probability of water maser presence. Therefore, from the current data we have been unable to derive an adequate model for water maser presence from dust clump radius.

5 CONCLUSION

We find water maser emission towards 128 of the 294 1.2-mm dust clumps searched. In total, we detect 165 distinct water maser sites and most are either new or achieve accurate positions for the first time.

There is an excellent correspondence between the positions of the water masers and the peaks of the 1.2-mm dust clumps in the majority of sources. In addition to the water masers that we detect towards our target 1.2-mm dust clumps, we detect four sources towards regions apparently devoid of dust continuum emission (from comparison between the water maser locations and the 1.2-mm continuum maps of Hill et al. 2005). We suggest that two of these sources may be located at the far distance which has resulted in lower sensitivity 1.2-mm continuum observations towards these sources.

Hill et al. (2005) allocated their 404 1.2-mm dust clumps in their catalogue the following categories: associated with a 6.7-GHz methanol maser; associated with both a methanol maser and 8-GHz radio continuum; associated with radio continuum only; and millimetre only, i.e. not associated with either methanol masers or radio continuum. We have assessed our detection rates of water masers towards the dust clumps in each of these categories. The highest water maser detection rates are towards dust clumps which are associated with methanol masers (both with and without radio continuum), and the lowest detection rate is towards the millimetre only sources (although at 23 per cent, this detection rate is still quite high). We additionally find that there are more dust clumps that are associated only with water masers (41) than those that are associated only with methanol masers (13). This suggests that water masers can be present at an even earlier evolutionary stage than methanol masers.

Comparison between the 1.2-mm dust clump properties with and without associated water maser emission shows (similarly to the results of Breen et al. 2007) that the water masers are associated with the bigger, more massive sources with higher peak and integrated flux densities. There is a trend whereby the more luminous water masers are associated with 1.2-mm dust clumps with lower H_2 number densities than those of the less luminous water masers. This trend is also seen in the case of both 6.7- and 12.2-GHz methanol masers (Breen et al. 2010a, 2011).

Like the 6.7- and 12.2-GHz methanol masers presented by Breen et al. (2011), we find that there is evidence for both the luminosity and the velocity range of the water masers to increase as the sources evolve. This implies that the gas volume conducive to the maser emission also increases with evolution. The water maser sources show evidence for this trend to 'turn over' towards the end of their lifetime, presumably showing a decline in both luminosity and velocity range until the emission ceases.

We have used these water maser observations to test the model for water maser presence towards 1.2-mm dust clumps presented in Breen et al. (2007). We find that there is a large number of water maser detections towards dust sources for which the computed probability of water maser presence is greater than 0.01, with a detection rate of 67 per cent towards these sources. However, since the number of clumps where we detect water maser emission (128) is higher than the number of clumps for which the probability of water maser presence is greater than 0.01 (58), it is clear that the model needs some refinement. The inadequacy of the current model may be (at least partially) attributed to the adoption of the near kinematic distance for sources where distance ambiguities exist, since an assignment of the far distance would result in a larger probability in sources where the water masers are detected.

We have attempted to create a new model for water maser presence towards 1.2-mm dust clumps, but find that we are severely limited by distance uncertainties. Our analysis shows that the prospects of creating a reliable model for water maser presence within 1.2-mm dust clumps is high when reliable distances can be assigned to the sources. Comparing the success of our model with that of Palla et al. (1991) shows that our model has much greater success in predicting water maser detectability.

A crude evolutionary implication of our derived model (in conjunction with the original model presented in Breen et al. 2007) is

that dust clumps with radii equal to 0.97 ± 0.29 pc (calculated using the difference between the radii threshold implied from each model) have a 50 per cent chance of forming one or more sources that are able to excite water maser emission. Although a simplistic view, this further implies that the lifetime of the dust clump is approximately twice that of water masers.

ACKNOWLEDGMENTS

We gratefully acknowledge many useful discussions with James Caswell which have increased the quality of the paper. The Australia Telescope Compact Array is part of the Australia Telescope which is funded by the Commonwealth of Australia for operation as a National Facility managed by CSIRO. This research has made use of NASA's Astrophysics Data System Abstract Service, the NASA/IPAC Infrared Science Archive (which is operated by the Jet Propulsion Laboratory, California Institute of Technology, under contract with the National Aeronautics and Space Administration), the SIMBAD data base, operated at CDS, Strasbourg, France, and data products from the GLIMPSE survey, which is a legacy science programme of the *Spitzer Space Telescope*, funded by the National Aeronautics and Space Administration.

REFERENCES

Batchelor R. A., Caswell J. L., Haynes R. F., Wellington K. J., Goss W. M., Knowles S. H., 1980, Aust. J. Phys., 33, 139
Beuther H., Walsh A., Schilke P., Sridharan T. K., Menten K. M., Wyrowski F., 2002, A&A, 390, 289
Braz M. A., Epchtein E., 1983, A&AS, 54, 167
Braz M. A., Scalise E., Jr, 1982, A&A, 107, 272
Breen S. L. et al., 2007, MNRAS, 337, 491
Breen S. L., Ellingsen S. P., Caswell J. L., Lewis B. J., 2010a, MNRAS, 401, 2219
Breen S. L., Caswell J. L., Ellingsen S. P., Phillips C. J., 2010b, MNRAS, 406, 1487
Breen S. L., Ellingsen S. P., Caswell J. L., Green J. A., Fuller G. A., Voronkov M. A., Quinn L. J., Avison A., 2011, ApJ, 733, 80
Caswell J. L., 1998, MNRAS, 297, 215
Caswell J. L., Breen S. L., 2010, MNRAS, 407, 2599
Caswell J. L., Phillips C. J., 2008, MNRAS, 386, 1521
Caswell J. L., Batchelor R. A., Haynes R. F., Huchtmeier W. K., 1974, Aust. J. Phys., 27, 417
Caswell J. L., Batchelor R. A., Forster J. R., Wellington K. J., 1983, Aust. J. Phys., 36, 443
Caswell J. L., Batchelor R. A., Forster J. R., Wellington K. J., 1989, Aust. J. Phys., 42, 331
Caswell J. L. et al., 2010, MNRAS, 404, 1029
Caswell J. L., Breen S. L., Ellingsen S. P., 2011, MNRAS, 410, 1283
Churchwell E., Walmsley C. M., Cesaroni R., 1990, A&AS, 83, 119
Codella C., Palumbo G. G. C., Pareschi G., Scappini F., Caselli P., Attolini M. R, 1995, MNRAS, 276, 57
Felli M. et al., 2007, A&A, 476, 373
Forster J. R., Caswell J. L., 1989, A&A, 213, 339
Genzel R., Downes D., 1977, A&AS, 30, 145
Green J. A. et al., 2010, MNRAS, 409, 913
Hill T., Burton M. G., Minier V., Thompson M. A., Walsh A. J., Hunt-Cunningham M., Garay G., 2005, MNRAS, 363, 405
Hofner P., Churchwell E., 1996, A&AS, 120, 283
Johnston K. L., Robinson B. J., Caswell J. L., Batchelor R. A., 1972, Astrophys. Lett., 10, 93
Kaufmann P. et al., 1976, Nat, 260, 360
Matthews H. E., Olnon F. M., Winnberg A., Baud B., 1985, A&A, 149, 227
Mookerjea B., Kramer C., Nielbock M., Nyman L., 2004, A&A, 426, 119
Palla F., Brand J., Comoretto G., Felli M., Cesaroni R., 1991, A&A, 246, 249
Palla F., Cesaroni R., Brand J., Caselli P., Comoretto G., Felli M., 1993, A&A, 280, 599
Sault R. J., Teuben P. J., Wright M. H., 1995, in Shaw R. A., Payne H. E., Hayes J. J. E., eds, ASP Conf. Ser. Vol. 77, Astronomical Data Analysis Software and Systems IV. Astron. Soc. Pac., San Francisco, p. 433
Smits D. P., 2003, MNRAS, 339, 1
Smits D. P., Cohen R. J., Hutawarakorn B., 1998, MNRAS, 296, L11
Sunada K., Nakazato T., Ikeda N., Hongo S., Kitamura Y., Yang J., 2007, PASJ, 59, 1185
Walsh A. J., Burton M. G., Hyland A. R., Robinson G., 1998, MNRAS, 301, 640
Walsh A. J., Lo N., Burton M. G., White G. L., Purcell C. R., Longmore S. N., Phillips C. J., Brooks K. J., 2008 Publ. Astron. Soc. Aust., 25, 105

This paper has been typeset from a TEX/LATEX file prepared by the author.